Biophysical Journal

Volume 112
Number 10

May 23, 2017

Biophysical Journal

www.biophysj.org

The Premier Journal of Quantitative Biology

Biophysical Society

Published by Cell Press
for the Biophysical Society

Biophysical Journal

Volume 112 Number 10 Pages 000–000 May 23, 2017

Biophysical Journal
Article

Biophysical Society

Long-Term, Stochastic Editing of Regenerative Anatomy via Targeting Endogenous Bioelectric Gradients

Fallon Durant,[1] Junji Morokuma,[1] Christopher Fields,[2] Katherine Williams,[1] Dany Spencer Adams,[1] and Michael Levin[1,*]

[1]Allen Discovery Center at Tufts University, and Department of Biology, Tufts University, Medford, Massachusetts; and [2]Independent Researcher, Sonoma, California

ABSTRACT We show that regenerating planarians' normal anterior-posterior pattern can be permanently rewritten by a brief perturbation of endogenous bioelectrical networks. Temporary modulation of regenerative bioelectric dynamics in amputated trunk fragments of planaria stochastically results in a constant ratio of regenerates with two heads to regenerates with normal morphology. Remarkably, this is shown to be due not to partial penetrance of treatment, but a profound yet hidden alteration to the animals' patterning circuitry. Subsequent amputations of the morphologically normal regenerates in water result in the same ratio of double-headed to normal morphology, revealing a cryptic phenotype that is not apparent unless the animals are cut. These animals do not differ from wild-type worms in histology, expression of key polarity genes, or neoblast distribution. Instead, the altered regenerative bodyplan is stored in seemingly normal planaria via global patterns of cellular resting potential. This gradient is functionally instructive, and represents a multistable, epigenetic anatomical switch: experimental reversals of bioelectric state reset subsequent regenerative morphology back to wild-type. Hence, bioelectric properties can stably override genome-default target morphology, and provide a tractable control point for investigating cryptic phenotypes and the stochasticity of large-scale epigenetic controls.

INTRODUCTION

Regeneration is thought to be a deterministic, robust process that precisely rebuilds the species-appropriate anatomical structures that are missing after significant injury (1). Here we show a striking counterexample illustrating that physiological manipulation can stably alter an animal's target morphology (the anatomical configuration that, once reached, causes regenerative growth and extensive remodeling to cease). Transformative advances in regenerative medicine will require understanding of the control systems that determine a given organism's large-scale anatomical pattern. Such controllers must integrate mechanisms over multiple scales, from molecular-level biochemical processes to system-level anatomical outcomes (2,3). To uncover biophysical epigenetic controls of body-wide patterning, we investigated the role of endogenous bioelectric signaling in this process in the highly regenerative planarian (*Dugesia japonica*).

Endogenous bioelectricity is an important emerging field (4–10). Numerous studies over the last century have characterized endogenous electric fields and ion currents that precede and predict important events in embryogenesis, regeneration, and cancer (10–19). Functional work has implicated developmental bioelectric states in the regulation of cell behavior such as proliferation, apoptosis, and differentiation (20,21), as well as tissue-level responses such as wound healing (22–25) and appendage regeneration (26–34). Recent advances have resulted in the establishment of molecular-genetic tools for manipulation of bioelectric signaling (35–38), and the integration of this biophysical, epigenetic layer of control with canonical signaling pathways and downstream transcriptional cascades (16,39–41). This field is also of significant importance for biomedicine, via the identification of numerous developmental channelopathies (42–44), the application of bioelectric signaling in cancer (36,45–48), and an appreciation of its role in stem cell bioengineering (49–53). It is becoming clear that endogenous voltage gradients are powerful, instructive cues that regulate growth and form (54). However, key questions remain about the bioelectric code—the mapping

Submitted January 20, 2017, and accepted for publication April 14, 2017.

*Correspondence: michael.levin@tufts.edu

Editor: Stanislav Shvartsman.

http://dx.doi.org/10.1016/j.bpj.2017.04.011

between stable (nonneural) electric states and subsequent anatomical outcomes.

Classical data in this field (55–58) addressed the ability of external electrical stimulation to reset the polarity of fragments in planaria—a system with extremely robust regenerative patterning. Recently, our group used biophysical (59–61) and computational (62–66) approaches to probe the fundamental issue of how pieces of planaria know which structures to make at which end. Here, we specifically test the hypothesis that bodywide bioelectric gradients serve as a kind of pattern memory (67)—an input into the integrated cellular decisions that allow the animal to recreate the same, invariant target morphology after damage and stop growth and remodeling as soon as that correct anatomy has been achieved. We also address the ubiquitous issue of variability, investigating in depth what happens to animals that seem to escape a particular experimental perturbation.

We found that altered bioelectric patterns underlie discrete, stochastic, and stable alterations to postregeneration axial polarity. Moreover, experimentally inverting the bioelectric signal rescued normal bodyplan anatomy, showing the bioelectric gradients to function as a bistable pattern memory switch that can reverse molecular-genetic commitment of axial polarity. We also uncovered a cryptic phenotype in animals that appear normal under molecular and histological assays but regenerate with a different pattern when cut due to their internal bioelectric state. This reveals that the bioelectric switch stores the pattern for future regeneration events within a currently normal anatomy. These experiments reveal a powerful instructive role for bioelectricity as a mediator of reprogramming of regenerative morphology.

MATERIALS AND METHODS

Colony care and sample sizes

A clonal strain of *D. japonica* was kept and maintained as in Oviedo et al. (68) and was starved for >7 days before cutting, a standard method used in this model system to reduce variability of data by controlling for the metabolic status of individuals (68). Planaria continued to be starved for the duration of the full experiment, which had no detrimental effect on regenerative ability or speed. Planaria at the start of each experiment were between 5 and 20 mm before being amputated into fragments. For each experiment, standard numbers of worms routinely used in the planarian literature were utilized to sufficiently capture significant differences given the amount of variation that is known to exist in each type of measurement.

Gap junction blockage and amputations

Amputations were performed as in Nogi and Levin (69). Fragments containing the pharynx were made using a sharp scalpel on a moistened and cooled Kimwipe (Kimberly-Clark, New Milford, CT) and piece of filter paper. Within 30 min of cutting, pharynx-containing fragments were transferred into an octanol solution (8-OH), prepared by slowly diluting 10 μL of 1-octanol (RM00050; Sigma-Aldrich, St. Louis, MO) into 500 mL of commercial natural spring water (Poland Spring, PS; Poland Spring Water, Framingham, MA) to a final concentration of 127 μM as in Oviedo et al. (70). 8-OH was left on a stir plate to mix for at least 30 min before treatment. 8-OH was remade and replaced daily for the first three days postamputation, then planaria were moved to PS in deep-dish plates (100 × 20 mm; Fisherbrand; Thermo Fisher Scientific, Waltham, MA) to regenerate in groups of 30 worms until day 21 before scoring and sorting. Sample sizes represented in text reflect pooled data from multiple replicates over the course of several months. Planaria were left at 20°C for the first seven days, then moved to 10°C to prevent fissioning.

Phenotype scoring

Scoring was performed under a model No. SV6 dissecting microscope (Carl Zeiss, Oberkochen, Germany). Criteria for a double-head (DH) phenotype were at least one eye on each side of the planarian. Criteria for a cryptic phenotype include at least one eye on the anterior side of the planarian, no eyes on the apparent posterior region, and no indication of other ectopic structures. The very rare (2.1%) regenerates that did not meet these scoring requirements developed an eyeless, radial body plan and were not analyzed further.

Secondary and tertiary amputations

Planaria were sorted according to phenotype after 21 days of regeneration and cut on the same cutting surface using the same tools as the first round of amputations. DH were amputated on either side of the two pharynxes. Heads and tail tips of similar size were removed from either side of the planarian and the remaining pharynx-containing fragments were allowed to regenerate in deep-dish plates until day 21 in PS until the next round of scoring, sorting, and subsequent amputation. Sample sizes represented in text reflect pooled data from multiple replicates over the course of several months. These experiments focus on the pharyngeal fragment rather than the pretail fragment found to produce 100% DHs in Oviedo et al. (70).

In situ hybridization

Animals were fixed in Carnoy solution for whole-mount in situ hybridization as in Nogi and Levin (69) for mature anterior tissue markers. For other probes, animals were formaldehyde-based fixed as in Pearson et al. (71). Probes used were: CNS marker PC2 (72), tail marker *Frizzled-T* (73), anterior markers *0821_HN*, *1008_HH* (74) (kind gifts from T. Gojobori), and anterior specification marker *ndk* (75).

Immunofluorescence and immunohistochemistry

Animals were fixed in Carnoy solution as in Nogi and Levin (69). For immunofluorescence, planaria were processed and imaged as in Reddien et al. (76).

Primary antibody: α-phosphorylated histone H3 (H3P), 1:250 (Upstate Chemical, Simpsonville, SC).

Secondary antibody: HRP-conjugated anti-Rabbit with TSA-Alexa568 anti-HRP (Molecular Probes, Eugene, OR).

Statistical analyses for immunofluorescence and immunohistochemistry

Tail-marker analysis: Expression levels were measured using a 450-pixel-area rectangular box drawn using FIJI software. Using the measure function, average gray values were recorded and compared. Statistical comparisons between head versus tail expression levels in wild-type (WT) and cryptic planarian individuals were made using the software Microsoft Excel (Microsoft, Redmond, WA) to calculate Student's *t*-test (two-tailed distribution, paired samples, unequal variance). Statistical comparisons between

tail expression levels in WT and cryptic planaria were made using Microsoft Excel to calculate Student's *t*-test (two-tailed distribution, unpaired samples, unequal variance).

Neoblast distribution analysis: A selection extending to 12% of the total length of the planarian on anterior and posterior ends was made using the software FIJI (National Institutes of Health, Bethesda, MD) and images were threshold adjusted to eliminate background fluorescence. Using the count function, the number of neoblasts within the selection was recorded and plotted over area. Area of the selection was calculated by converting pixel area to mm^2 using scale bars as reference. The neoblast density, measured in number of neoblasts/mm^2, was calculated in Microsoft Excel. Statistical comparisons of neoblast density were made using Microsoft Excel to calculate Student's *t*-test (two-tailed distribution, unpaired samples, and unequal variance).

Membrane voltage-altering pharmacological treatments and amputations

SCH-28080 (Sigma-Aldrich) treatments were performed as in Beane et al. (60). DH were amputated on either side of the two pharynxes then soaked in SCH-28080 as described. DMSO-treated controls had no effect and DH phenotype remained persistent. Sample sizes were pooled from three technical replicates.

Membrane voltage reporter assay

Bis-[1,3-dibarbituric acid]-trimethine oxanol ($DiBAC_4(3)$; Invitrogen, Carlsbad, CA) was used as in Adams et al. (33) and Oviedo et al. (77). Planaria were amputated to produce pharynx-containing fragments as above; these fragments were then soaked in PS or 8-OH solution. Planaria regenerated for at least 21 days when they were scored and sorted according to cryptic or DH guidelines above. Whole planaria were soaked in $DiBAC_4(3)$ solution for >30 min before imaging and were immobilized using 2% low-melting point agarose and Planarian Immobilization Chips (78). WT and cryptic regenerates were mounted ventralized and, whenever possible, imaged on the same chip in tandem so that direct comparisons of bioelectric physiology could be made. Animals were tracked individually in multiwell, non-treated cell culture plates (12-well; Falcon/Corning, Corning, NY) then reamputated following the procedure in Secondary and Tertiary Amputations. Functionality of $DiBAC_4(3)$ as a voltage reporter (33,60,61,77,79–84) was reconfirmed by imaging and comparing WT worms with animals soaked in a 1 μM valinomycin + 150 mM potassium gluconate (valinomycin + KGluc) depolarization solution (see Fig. S5 for data and analysis). Voltage profiling data are limited to the outermost few cell layers, as the depth of dye imaging is limited to, at most, ~50 μm due to opacity and pigmentation of planaria tissues.

Image collection and processing

Membrane voltage (V_{mem}) images were collected using a model No. AZ100 Stereomicroscope (Nikon, Melville, NY) with a model No. DL-604M VP camera (Andor Technology, South Windsor, CT), using an epifluorescence optics FITC filter (GFP HC: 470/40, 495, 525/50), and pseudocolored images were created using the NIS-Elements imaging software (Nikon). V_{mem} images were flat-field corrected using the software MetaMorph (Molecular Devices; https://www.moleculardevices.com/systems/metamorph-research-imaging). All other images were collected using a model No. SMZ1500 microscope (Nikon) with a Retiga 2000R camera (Qimaging, Surrey, BC, Canada) and Q-Capture imaging software (Qimaging). Adobe Photoshop (Adobe Systems, San Jose, CA) was used to organize figures, rotate and scale images, and improve visibility of entire image with the exception of the V_{mem} images. Quantitative analysis was performed using the software FIJI, with neoblast counting using the threshold function and bioelectric analysis using the measure function. Data were neither added nor subtracted; original images available upon request.

Statistical analysis for phenotypic data

State diagram: The ratio of DH to cryptic morphologies across all experiments was close to 25:75%. The statistical significance of departures from the fixed 25:75% ratio shown in the state diagram (Fig. 5) was made using Microsoft Excel to calculate Student's *t*-test (two-tailed distribution, unpaired samples, unequal variance).

SCH-28080: Error bars for % phenotypes were calculated using 95% confidence intervals.

Statistical analyses for bioelectric physiology

A box with area proportional to 10% of the length of the planarian was drawn in the anterior and posterior regions of both WT and cryptic planaria. Using the measure function in the software FIJI, average intensity values within the box were recorded. Statistical comparisons between WT and cryptic tails, as well as between WT and valinomycin + KGluc-treated animals, were made using Microsoft Excel to calculate Student's *t*-test (two-tailed distribution, paired samples, unequal variance).

Predictive modeling

A quantitative model of the stochastic branching between cryptic and DH morphologies across multiple rounds of regeneration was implemented using JavaScript (https://www.javascript.com/) and the HTML5 canvas function. The model can be manipulated and its source code examined at http://chrisfieldsresearch.com/GJ-memory-model.htm. For model equations, see Fig. S6.

RESULTS

Editing the bioelectrical network stably alters regenerative morphology to a stochastic outcome

Planaria exhibit extensive regenerative capacity, where each fragment regenerates precisely what is missing to complete a planarian-specific anatomy (i.e., target morphology) (85–87). Given the widespread biological use of bioelectric circuits for memory (88,89) and the control of embryonic organ identity by endogenous voltage gradients (10,67,90), we investigated the role of bioelectric signaling in regenerative pattern memory. Bioelectric signals are changes in the spatio-temporal pattern of slowly changing (steady-state) endogenous anatomical gradients of resting potentials across many tissue types (6,10). Bioelectric circuits in neural and nonneural tissues employ electrochemical synapses known as gap junctions (GJ) (91). In planaria, gap junctional communication (GJC) via innexins and specific V_{mem} signals are required for proper anterior-posterior (A/P) polarity (60,69,70). Because planaria are not amenable to channel misexpression technology, and because RNAi approaches do not allow transient modulation, we exploited a pharmacological tool that can target electrical synapses in a transient manner. We utilized 8-OH, a widely used GJ blocker (92,93), to alter the dynamics of the bioelectric network in planarian fragments. Exposure to 8-OH reduces the ability

of cells to communicate ionically, partially fragmenting the long-range circuit and resulting in a greater number of smaller adjacent isopotential domains (shown and analyzed in (59)).

Treatment of trunk fragments (planaria that have had their heads and tails amputated) with 8-OH disrupts A/P polarity producing a DH phenotype, without toxicity, mutagenic effects, or changes in neoblast maintenance (70) (Fig. 1 *A*). 8-OH treatment phenocopies the gene-specific knockdown of three innexins (70), which also produces the exact same biaxial DH outcome. But unlike injection of RNAi, which cannot be removed or turned off, our method allows testing for persistent effects: although it efficiently blocks GJC and thus effectively increases the number of distinct, smaller adjacent regions of unique V_{mem} (isopotential domains) (59), 8-OH is known by GC-MS analysis to efficiently wash out of worm tissues in 24 h (70). The most remarkable aspect of the DH phenotype induced by a 48 h 8-OH GJC disruption, is that it is, in the absence of further treatments, permanent: both heads can be removed, the middle fragment can be allowed to regenerate, and the heads removed again multiple times, over months until the worms are too small to cut, in plain water long after the original drug is gone. Yet, the DH morphology recurs in perpetuity (Fig. 1 *B*), even after spontaneous fission in plain water—the animals' most common reproductive mode (see Fig. S1 *B*), as well as after any additional subsequent rounds of 8-OH treatment (100%, $N = 100$). Thus, species-specific axial pattern can be overridden by briefly changing the connectivity of a physiological network. This finding left several key open questions. Can the physiological state regulate molecular-genetic machinery that normally establishes a tail at the posterior and, and if so, is there a short window of competence for this effect? What stable property mediates the information needed for a fragment to decide to make one head or two? Why do some animals escape the effects of 8-OH exposure and regenerate single-headed (SH)? And finally, can DH worms ever be reset back to normal? Here, we addressed these unknowns in this fascinating model system.

Importantly, the effects of 8-OH exposure do not convert all of the animals in an experimental cohort (*CRPT*; Fig. 1 *A*)—they exhibit differential responses, even though they are clonal individuals. Upon treatment with 8-OH

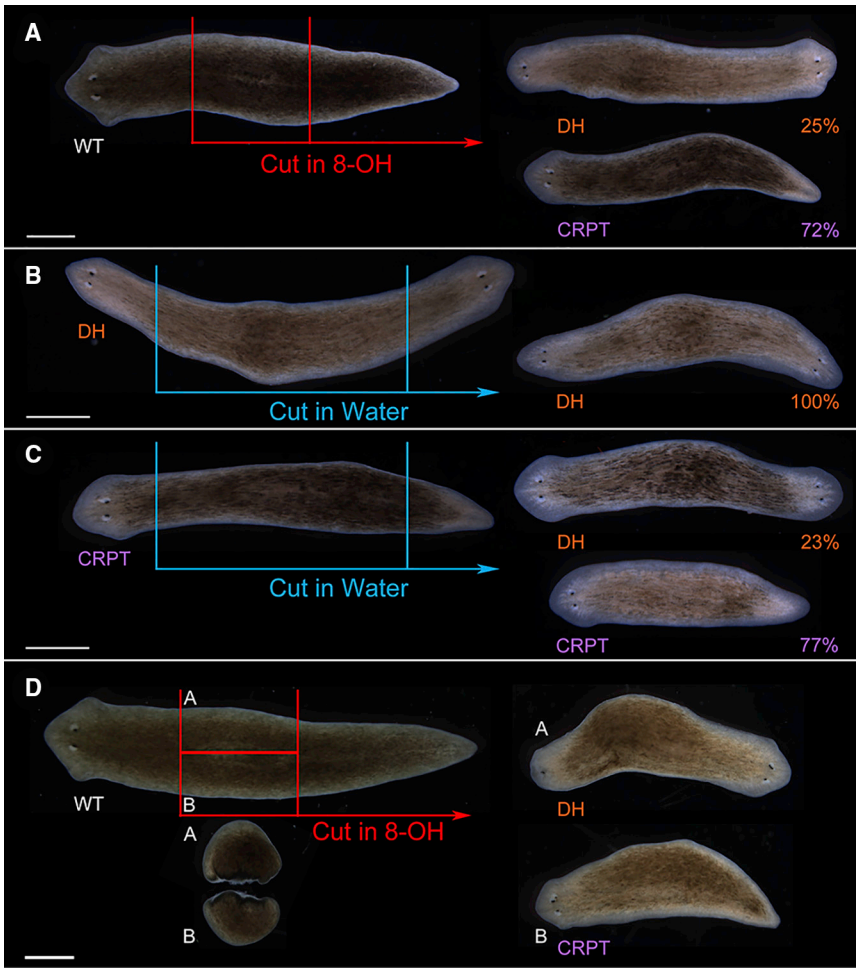

FIGURE 1 Current morphology does not necessarily represent target morphology. Representative phenotypes following GJ blocker or water treatment are shown. Conditions: (*A*) WT *D. japonica* pharyngeal fragments treated in 8-OH 21 days postamputation, 72% cryptic (CRPT), 25% DH ($N = 573$). (*B*) Twenty-one days postamputation, DH *D. japonica* created from pharyngeal fragments treated in 8-OH were recut in water. Heads were completely removed past the auricles on each side in equal amounts, 100% DH ($N = 100$). Left side DH trunk fragment regenerated the DH shown on the right. (*C*) Twenty-one days postamputation, *D. japonica* cryptic planaria created from pharyngeal fragments treated in 8-OH were recut in water. Head was completely removed past the auricles on anterior side, and an equal amount was removed from the posterior side, 77% cryptic ($N = 155$), 23% DH ($N = 155$). Left side cryptic fragment regenerated the DH shown on the right. Right side cryptic regenerated from another parent cryptic planarian not shown. (*D*) WT *D. japonica* pharyngeal fragments after an immediate, subsequent transverse amputation can regenerate independent patterning fates (both DH and cryptic). Scale bars represent 1 mm. To see this figure in color, go online.

($N = 593$), trunk fragments produce 25% DH planaria, 72% planaria with normal SH A/P polarity (CRPT), and ~3% planaria with indiscriminate shapes lacking eyes completely. At first we considered the morphologically normal planaria resulting from 8-OH treatment to be escapees—those that failed to be affected by the treatment, as this kind of partial penetrance is observed with practically every functional protocol in most published studies. We then asked: were these animals really escapees, or might control circuits have been altered in a way that is not yet apparent? Remarkably, when morphologically normal regenerates were amputated again, in plain spring water, as long as eight weeks after the original amputation in 8-OH, it was discovered that they were in fact not normal with respect to their regenerative outcomes: 23% ($N = 155$) regenerated as DH planaria (Fig. 1 *C*) with true, duplicated anterior structures (Fig. S2). DH worms were similarly obtained from fragments taken posterior to the pharynx, ruling out the necessity of a specific body region (or one having multiple pharynxes) for producing the DH phenotype in subsequent generations. Thus, morphologically normal cryptic planaria clearly did not escape the effects of 8-OH, but their alteration is not apparent in the intact state: their altered pattern memory is revealed only upon regeneration, despite their normal anatomical phenotype. Thus, the SH cryptic fraction resulting from 8-OH treatment are not WT (which would regenerate as 100% SH) but are altered so as to generate the same proportion of SH and DH forms upon multiple subsequent rounds of cutting in plain water (Fig. S3).

It has been reported that very thin fragments sometimes regenerate DH planarians in water spontaneously (94); however, these fragments were of standard experimental size normally seen in the field, which never spontaneously regenerate DHs. Although biaxial DH phenotypes have been reported classically as so-called "heteromorphoses" (95), and the persistence of DH memory has been shown (70), this is to our knowledge the first situation in which completely normal-seeming worms will regenerate to a radically different bodyplan upon amputation in plain water: target morphology (the form to make upon future injury) can be edited to be different than current morphology, despite the normal high degree of robustness in this highly regenerative species.

Furthermore, the phenotype is stochastic, in the sense that discrete outcomes occur in predictable ratios within a treated population, but individual animals (though clonal and living in the same environment) regenerate toward distinct outcomes despite identical experimental perturbation. To test whether the stochastic ratio of anatomical outcomes could be changed by a second exposure to 8-OH, a separate cohort of cryptic planaria was generated according to protocol and was amputated, but this time treated in 8-OH a second time. Again, the same stochastic ratios were seen, 24.5% ($N = 439$) DH and 75% ($N = 439$) had normal morphology. Approximately 0.5% regenerated indiscriminate shapes without eyes ($N = 439$). We further confirmed this anatomical coin-toss by testing adjacent pieces of a cryptic worm that came from the same A/P level. We found that the stochastic decision to become DH or cryptic is made independently by each fragment, rather than determined by some property of the parent worm, as exhibited by the ability of two transverse pieces of a WT worm fragment to develop two completely different patterning fates after 8-OH treatment (Fig. 1 *D*).

To our knowledge, no data have been available on the stochastic nature of anatomical reprogramming. One key requirement of such a system is that it directs downstream activity of the genetic programs that establish head and tail structures. We found that even after posterior identity at the tail-facing wound is established at the transcriptional level, anatomical specification can be reversed by subsequent instructive physiological signals, which respecify both the molecular and the anatomical state of the new tissue (Fig. 2). More importantly, however, the new stochastic

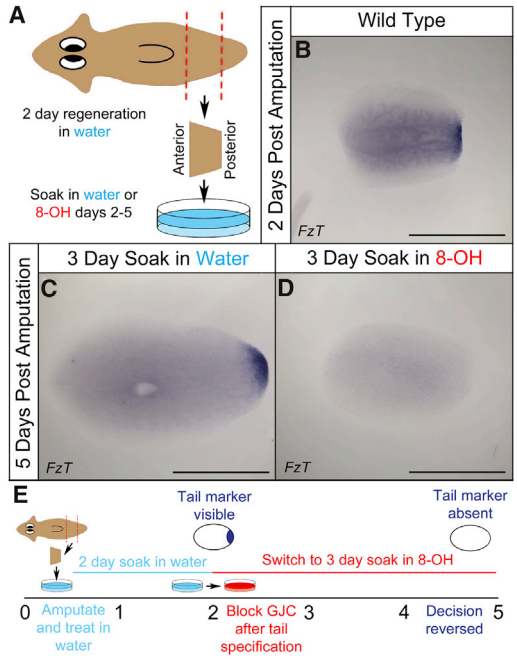

FIGURE 2 Transient GJ inhibition overrides expression of early posterior markers. (*A*) Planaria were allowed to regenerate for 2 days in water before they were exposed to a late 3-day treatment in 8-OH. (*B*) Two days postamputation, WT *D. japonica* express early tail markers (*FzT*) at the posterior blastema (100%, $N = 10$). (*C*) Five days postamputation, WT *D. japonica* continue to express tail markers at the posterior end over a wider area (100%, $N = 10$). (*D*) If planaria are treated in 8-OH from days 2–5, after the posterior genetic program is initiated (see *B*), tail marker expression is no longer visible at 5 days (30%, $N = 10$) or diminished (30%, $N = 10$). (*E*) Timeline of late 8-OH treatment. Planaria are amputated and soaked in water for two days, at which point tail markers become visible. GJC is inhibited after tail specification using a 3-day soak in 8-OH from days 2–5. By day 5, the decision is reversed and tail markers are no longer visible. Scale bars represent 1 mm. $n \geq 10$ for each. To see this figure in color, go online.

DH pattern has to be somehow stored within the body of cryptic planaria, so that it can guide the results of subsequent regeneration. What stable histological, cellular, molecular, or physiological state distinguishes true WT planaria from normal-looking (SH) cryptic planaria?

Target morphology is not stored via mature tissues, key early anterior mRNA expression, or neoblast distribution

Cryptic worms were indistinguishable from normal worms with respect to a number of key molecular properties, in addition to their normal anatomy. Cryptic planaria did not have internal mature anterior structures that could have triggered regeneration of a second head upon amputation. All DH planaria (100%, $N = 5$) exhibited strong expression in both heads of head tissue markers including PC2 (72), 0821_HN, and 1008_HH (74), which are expressed by the central nervous system, the sensory cells of the anterior fringe, and brain branches, respectively (Fig. 3, *C*, *F*, and *I*). In contrast, cryptic planaria (100%, $N = 5$), like WT, only exhibited expression of anterior tissue markers at the single anterior end (Fig. 3, *B*, *E*, and *H*), showing that cryptic planaria have normal histological A/P polarity (Fig. 3, *A*, *D*, and *G*).

Likewise, cryptic planaria did not have aberrant expression of early anterior driver genes in their posterior ends. Focusing on the most essential candidate, we examined *ndk*, one of the earliest anterior specification markers in the planarian (75), commonly used in various planarian species (96–99) due to its function of regionalizing where brain tissues may form (75). WT planaria cut and regenerated in water express *ndk* robustly and only in the anterior region where the cephalic ganglion resides (100%, $N = 13$; Fig. 3 *J*). Likewise, SH cryptic planaria also only expressed *ndk* in the most anterior region (100%, $N = 10$; Fig. 3 *K*). Positive control DH worms expressed *ndk* robustly at both ends (100%, $N = 10$; Fig. 3 *L*). Thus, the regeneration of cryptic planaria as DH is not due to ectopic presence of early essential head-specific mRNA such as *ndk*, although it cannot be ruled out that differences could be found by future studies using as-yet undiscovered anterior determinant genes.

To test whether cryptic planarians' posterior ends might be destabilized due to failure to express required tail

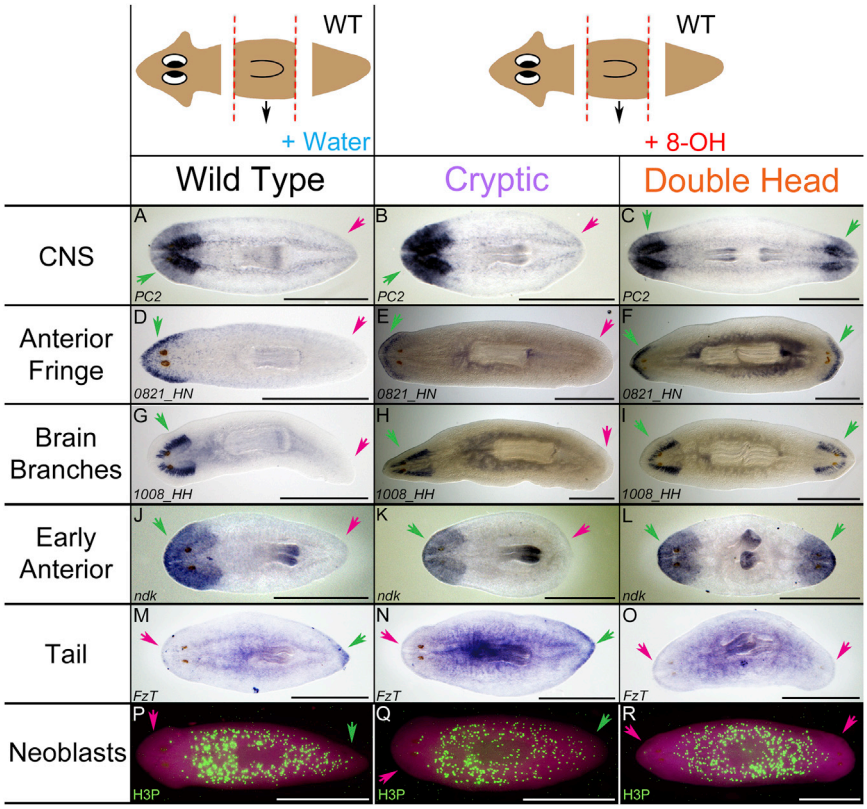

FIGURE 3 Target morphology is not stored via mature tissues, candidate early anterior mRNA expression, or neoblast distribution. Tissue-specific analyses were performed at 21 days postamputation. $n \geq 5$ for each. WT *D. japonica*, cut and treated in 8-OH (127 μM), went on to regenerate a population of DH and a population of cryptic planaria. These were compared to WT *D. japonica* cut and treated in water as a control. Regions showing expression pattern are indicated using green arrows. Regions devoid of expression pattern are indicated using pink arrows. (*A* and *B*) WT and cryptic planaria express *PC2* CNS marker robustly in the brain and ventral nerve cords that extend to the tip of the tail whereas (*C*) DH planaria express PC2 robustly in a bipolar fashion at each end of the worm. (*D*), (*E*), (*G*), and (*H*) WT and cryptic planaria also express mature anterior fringe tissues (*0821_HN*) and brain branches (*1008_HH*) only in the head, not in the tail, whereas (*F*) and (*I*) DH express these robustly at each end of the worm. (*J* and *K*) WT and cryptic planaria are also only limited to robust *ndk* expression throughout the head region. (*L*) Conversely, DH planaria express the early anterior mRNA *ndk* robustly at both ends. (*M*) WT planaria express *FzT* tail marker significantly near the tail tip as compared with the anterior tip ($p = 0.0001$, two-tailed, paired Student's *t*-test). (*N*) Similarly, cryptic planaria also significantly express *FzT* tail marker near the tail tip as compared with the anterior tip ($p = 0.0004$, two-tailed, paired Student's *t*-test) and is not statistically different from expression seen in WT ($p = 0.6313$, two-tailed, unpaired Student's *t*-test). (*O*) DH *FzT* expression comparing the two heads was not statistically significant ($p = 0.4079$) All expression levels for *FzT* were quantitatively measured for comparison using raw images (450 pixel area, measured function of *shaded values*; FIJI software used). (*P* and *Q*) WT and cryptic *D. japonica* are devoid of neoblasts (H3P immunohistochemistry, all planes and neoblasts visible) in the region anterior to the eyes. Neoblasts begin immediately posterior to the eyes and extend to the tip of the tail. (*R*) DH have this region devoid of neoblasts on both sides of the worm. Overall, cryptic planaria, in terms of these markers, are more similar to WT than to DH despite the fact that 25% will go on to regenerate DH. Scale bars represent 1 mm. To see this figure in color, go online.

markers, we probed the expression of *frizzled-T* (*FzT*), a key Wnt receptor gene involved in specification of the posterior region (100); in addition to obvious qualitative differences, we also quantified the spatial distribution of the in situ hybridization signal. WT planaria showed the expected significant difference in expression of *FzT* between heads and tails ($p = 0.0001$; Fig. 3 *M*). Similarly, cryptic planaria had significantly higher expression of *FzT* in tails compared to heads ($p = 0.0004$; Fig. 3 *N*). Consistently with this, the difference in FzT expression between the two heads of DH worms was not statistically significant ($p = 0.4079$; Fig. 3 *O*). There were no statistically significant differences in expression of *FzT* between WT and cryptic planaria ($p = 0.74$, Fig. S2). Thus, cryptic worms' posterior ends are true tails indistinguishable from WT tails by expression of *FzT*; their altered regenerative pattern is not due to a lack of tail identity.

Neoblasts in WT and DH *D. japonica* are absent from the region anterior to the photoreceptors (Fig. 3, *P* and *R*) (101). If abnormal target morphology was stored in cryptic planaria via headlike distribution of neoblasts in the posterior structures, this would be revealed by a lack of proliferating cells near the tip of the posterior region of cryptic planaria. The distribution of mitotically active cells in cryptic tails using the standard H3P marker (76) did not resemble the anterior neoblast distribution (Fig. 3 *Q*). In cryptic planaria, the anterior neoblast density significantly differs from that in the posterior tip ($p << 0.0001$ for each; Fig. S4), whereas differences in average neoblast density between WT and cryptic tails were not statistically significant ($p = 0.3369$). This confirms that the neoblast distribution in the cryptic worms' tails is not headlike. Thus, cryptic planaria do not maintain their unique regenerative response via a head-specific distribution of neoblasts in posterior tissues.

Cryptic planaria have different bioelectric physiology from normal planaria

Bioelectric prepatterns regulate cell behavior and developmental pattern formation (42,60,61,84,102). We hypothesized that cryptic planarians' DH regenerative target morphology could be stored via a change in the bodywide distribution of cellular resting potentials, especially because 8-OH has been shown to alter bioelectric prepatterns by generating more isopotential regions of V_{mem} patterning in planaria (59). Using $DiBAC_4(3)$ voltage reporter, a well-established dye used for characterization of V_{mem} signatures of patterning systems in vivo (33,59,60,77), we observed that mature WT worms have a relatively depolarized anterior region (Fig. 4 *A*). Crucially, cryptic planaria exhibit a second (ectopic) region of depolarization near the posterior end, including the tail (Fig. 4 *B*). WT and cryptic planaria were imaged in $DiBAC_4(3)$ together in the same field to enable direct comparison of relative V_{mem} signatures in a pairwise analysis.

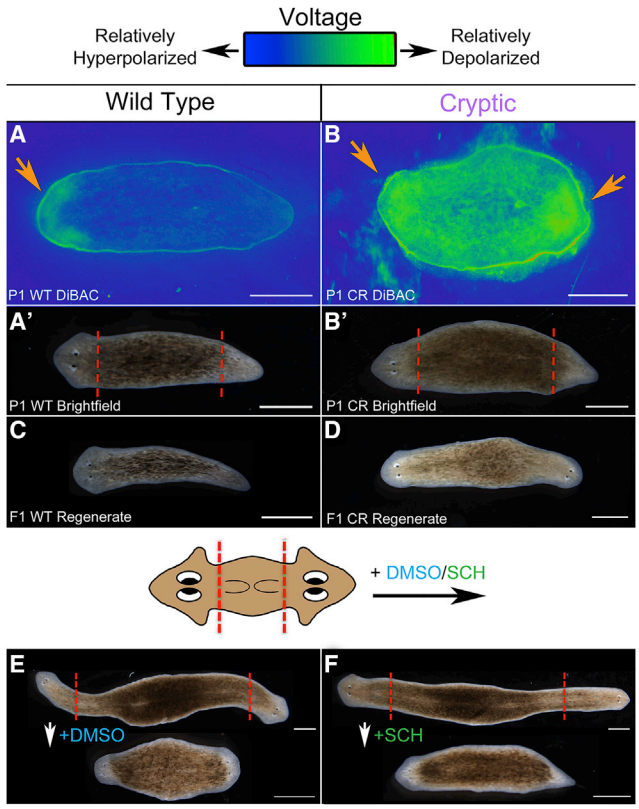

FIGURE 4 Cryptic planaria have differential bioelectric physiology. (*A* and *B*) V_{mem} reporter assay using $DiBAC_4(3)$. Images are pseudocolored blue-green. Brighter pixels (*green*) are more relatively depolarized or positively charged on the inside of cells relative to the outside. Pixels of lower intensity (*blue*) are more relatively hyperpolarized or negatively charged on the inside of cells relative to the outside. (*A*) WT *D. japonica*; anterior cells, particularly around the region of the auricles (*orange arrow*), are more relatively depolarized than posterior cells. (*B*) Cryptic planaria also have relatively depolarized anterior cells, especially around the auricles (*left orange arrow*) but also have a region of relative depolarization at the tail (*right orange arrow*) that is not present in the tail region of WT. (*A′* and *B′*) Bright field images of animals shown in (*A*) and (*B*), respectively. Planaria were cut according to the diagrams shown. (*C* and *D*) Resultant regenerates from amputated planaria represented in (*C*) and (*D*). (*C*) A WT regenerate produced a planarian with normal polarity after $DiBAC_4(3)$ analysis. (*D*) Cryptic planaria regenerate a DH phenotype after $DiBAC_4(3)$ analysis. (*E*) The DH phenotype can be reset with bioelectric manipulation. Planaria that are DH after 8-OH treatment exhibit a permanent change in target morphology. When soaked in DMSO upon recutting, planaria consistently remain DH even after three generations of recuts (100%, $N = 102$). (*F*) DH planaria, recut and treated in hyperpolarizing H,K-ATPase inhibitor SCH-28080 show a permanent reset of the target morphology back to the SH phenotype (34%, $N = 102$). Scale bars represent 1 mm. To see this figure in color, go online.

After V_{mem} analysis, WT and cryptic planaria were brightfield imaged and recut (Fig. 4, *A′* and *B′*). $DiBAC_4(3)$ exposure had no effect on WT planarian polarity (Fig. 4 *C*) and correctly indicates depolarization as verified using a depolarizing treatment consisting of the potassium ionophore valinomycin and potassium gluconate (Fig. S5; (42,60,77,79–81,103,104)). Cryptic planaria that regenerated DH upon

recutting (Fig. 4 *D*) all had shown regions of relative depolarization at the posterior end compared to their paired controls ($p = 0.025$; Table S1). Similarly, unlike WT tails that are significantly more hyperpolarized than WT heads ($p < 0.01$), cryptic tails are not significantly different from cryptic heads ($p > 0.05$). These measurements specifically focused on animals that went on to form DHs, to understand what was different about the worms that would change their anatomical layout upon cutting. This significant relationship reveals a physiological signature that, unlike the other tested properties, reveals what changed in the cryptic planaria: they have a headlike bioelectric state, in at least the surface tissues of their posterior end, which could be responsible for the DH regeneration outcome. These data show that bioelectric state is a unique marker of altered target morphology in anatomically and molecularly normal planaria, which would reveal, to our knowledge, their novel regenerative pattern upon future rounds of amputation.

The above data suggest a specific manipulation for altering the encoded target morphology. To test the instructive, functional role for the voltage gradient we observed, we asked: can the persistent DH morphology be rewritten back to a normal WT condition by manipulation of V_{mem} gradients? The alteration of subsequent rounds' animals' target morphology induced by changes of bioelectric connectivity predicts that directed manipulation of resting potentials (4,10,59–61,63,67,105–107) could be used to reverse the worms' altered anatomical outcomes. Is the circuit we observed a true bistable pattern memory switch?

No gain-of-function (misexpression) technology exists for planaria; thus dominant channel misexpression (used in other model systems for control of developmental bioelectricity (35,108)) was not feasible. We exploited the rich pharmacological toolkit that exists for modulating bioelectric state by regulating native ion conductances (34). The H,K-ATPase ion pump inhibitor SCH-28080, validated by gene-specific knockdown of H,K-ATPase by RNAi, have been shown to robustly hyperpolarize planarian tissues, as confirmed with $DiBAC_4(3)$ imaging (61); inhibit head identity in amputated fragments; and suppress ectopic head formation even in the presence of otherwise DH-producing β-catenin RNAi (60). However, the effects of hyperpolarization have never been explored in the context of permanent (multigeneration) DH phenotypes. Thus, we sought to determine whether we could reset target morphology back to normal from the most extreme example of revised target morphology, the persistent DH state. We observed that 34% of DH planaria ($N = 102$; Fig. 4 *F*) cut and treated with SCH-28080 exhibited normal SH regeneration, which was persistent across multiple generations, unlike controls in vehicle (DMSO) that continued to regenerate as DH (100%, $N = 102$; Fig. 4 *E*). Similarly, after hyperpolarization with SCH-28080, the rate of cryptic worm conversion to the DH phenotype postamputation was reduced to 1% ($N = 100$). In all cases, the stable outcome was WT (SH worms that only give rise to SH worms in subsequent generations), not cryptic. These functional results confirm the voltage relevance of our dye pattern: the bioelectric method and data correctly predicted and identified a functional treatment that efficiently resets the DH state back to normal.

Most crucially, this was not a transient suppression, but was stable reprogramming: the resulting SH phenotype remained persistent after at least four consecutive generations of recuts (34%, $N = 102$; Fig. S1 *C*). All control planaria cut and treated in vehicle (DMSO) remained DH across all generations of recuts (100%, $N = 102$; Fig. S1 *A*). Thus, the altered regenerative anatomical pattern encoded in the planarian body can be forced back to a WT state by resetting the bioelectrical circuit—the stable voltage prepattern is functionally determinative of regeneration outcome.

DISCUSSION

> "The so-called 'polarity' exhibited in the regeneration of animals has suggested the idea … that the phenomenon might be related to the outcome of differences in potential in different regions; or, in other words, of electrical polarity. … If this relation should be found to exist, there is a further opportunity of testing the validity of the conclusion in the case of axial heteromorphosis."
>
> —T. H. Morgan (95)

Even in genetically identical populations, individuals can exhibit heterogeneous phenotypes that could increase fitness in changing environments (109), drive decisions regarding cell fate and lineage (110), or lead to differences in overall shape (59). Several studies (reviewed in (111)) have shown that target morphology, or pattern memory, can be manipulated, but no endogenous control mechanisms are known. Here we show that transient inhibition of GJC permanently alters the shape to which planaria will regenerate, via a stochastic mechanism involving a stable bioelectric prepattern. This bioelectric prepattern exists at least in the surface tissues of the worm; future development of transgenesis and tissue-specific promoters in planaria will exploit genetically encoded voltage reporters to probe which cell types store the bioelectric state.

The outcomes of planarian regeneration in each of the observed stable configurations that result from GJ network perturbation are summarized in a state transition diagram (Fig. 5). The DH state is a terminal node; worms that regenerate as DH never spontaneously go back to a cryptic or WT SH state. However, DH worms can be forced back to a SH state, and the transition probability of cryptic worms to DH is almost eliminated by exogenous control of resting potential, illustrating that the observed bioelectric depolarization inherent in cryptic worms is a functional determinant of anatomical outcome. It is possible that additional modalities for rewriting the target morphology

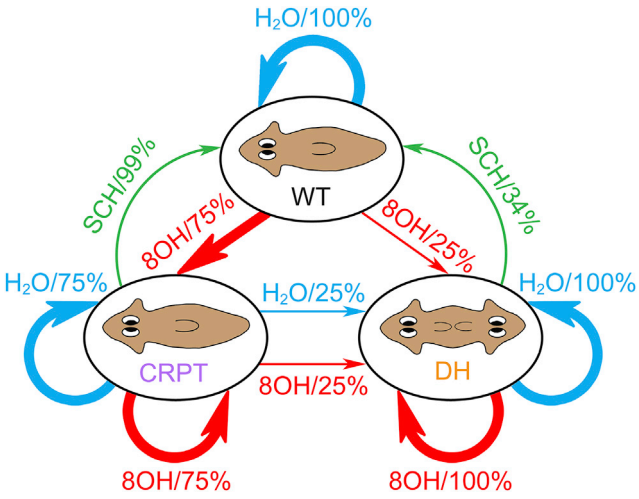

FIGURE 5 Change in target morphology is stable and stochastically variable. The percentage of phenotype, CRPT (cryptic/SH) or DH (double head), was recorded from pharyngeal fragments that were treated in GJ blocker (8-OH), H,K-ATPase inhibitor (SCH-28080), or water. The DH phenotype remains permanent, but cryptic planarian regeneration is stochastic, resulting in a 75:25 ratio of SHs to DHs in both water and 8-OH treatments. To see this figure in color, go online.

will be uncovered in future work; it is likewise possible that <100% penetrant phenotypes reported throughout the literature might also reflect other interesting cryptic effects, which remain to be tested by challenging the escapees in subsequent experiments. The identification of reagents that permanently rewrite the target morphology, and insight into the mechanisms underlying such a change, have until now been hampered by the stochastic, cryptic nature of this change (apparent escapees) and the robust fidelity of the regenerative program in the planarian under most manipulations. To our knowledge, these data are the first demonstration in a metazoan organism of significant changes to the body plan that are stable, stochastic, and induced by a brief and purely physiological perturbation.

These findings significantly advance our prior work. Beane et al. (60) showed that depolarization is able to induce head formation in posterior facing wounds in one round of regeneration; it was unknown whether this was stable (permanent) or transient. In contrast, the above data show voltage change to be sufficient to permanently reset a stable change in the target morphology (the cryptic phenotype) rather than merely affecting the WT state. Oviedo et al. (70) showed that DH state can be permanent; however, that study (and those from all other labs) count normal-looking worms as merely indicative of a less-than-fully penetrant phenotype. In contrast, we show that this instead reveals a subtle and profound change to the animals' pattern memory. Lastly, we now show that bioelectric change can override molecular tail identity even after tail marker is expressed (Fig. 2).

Given that the voltage change induces complete second heads and resets the DH phenotype to produce tails, it is very likely that these instructive voltage changes lie upstream of the endogenous gene networks that are needed to build a head (86). Bioelectric signaling operates in concert with downstream target genes and chromatin modifications. Thus, it is likely that additional components of the DH effect may include other epigenetic mechanisms that integrate with bioelectrics to define outcomes above the cell level. Current molecular models have implicated Wnt signaling as a key regulator of A/P polarity (reviewed in (112)); however, these models are currently unable to explain the multigenerational persistence of the DH phenotype, the nature of stochasticity or escapees of a given treatment, and the ability of target morphology to be reset by bioelectric manipulations. Regardless of the putative genes or epigenetic mechanisms that may be involved, we found a way to simply bypass the molecular genetics that influence polarity by altering endogenous distributions of resting potential. This is attractive in translating this work to regenerative medicine because bioelectric physiology is a much easier target for treatment than genetic manipulation.

We suggest a model that correctly predicts the ratio of cryptic to DH worms for the manipulations performed (Fig. S6). This model attributes the emergence of the cryptic state to the breakdown of an organism-wide, GJ- and polarization-dependent axial pattern memory that continuously amplifies the probability of normal, WT morphology as the dominant target morphology in the event of injury. It assumes that this pattern memory is implemented by cellular response to a signal transmitted from anterior to posterior. The consistently correct regeneration of WT animals would be the result of active, ongoing suppression by this memory signal of the stochasticity that would be observed if target morphologies were allowed to compete on a level playing field. The model postulates two effects of briefly disrupting GJ function with 8-OH treatment after an amputation: 1) memory signal reception is disrupted immediately at the anterior wound by the amputation, and slowly at the posterior wound by the disruption of GJ-dependent signal transmission, leading to stochastic competition between head and tail pathways at the posterior wound; and 2) both regenerated heads and regenerated tails are depolarized relative to the middle of the animal. Stochastic competition between pathways produces DH worms, whereas the depolarized tail prevents the WT pattern memory from being reestablished after regeneration, producing the cryptic phenotype. The depolarized tail of cryptic worms disrupts anterior to posterior transmission of the memory signal; hence head and tail pathways compete stochastically at both wounds after further amputations. Externally polarizing the tail of a cryptic worm reinitiates anterior to posterior transmission of the memory signal, restoring WT response to further amputations as observed. As recognized from Turing (113) onward, the implementation of memory signals such as

postulated here requires dynamic interaction, either in the form of competition between short- and long-range signals (114), resonance as implemented in many neural network models (115), enzymatic amplification of reaction rates, or some other energy-consuming process. Our current efforts are aimed at integrating this model and its stochastic dynamics with the recently developed bioelectric simulator environment (116). We are constructing a comprehensive, realistic model comprising the known physiology, gene-regulatory networks, and biochemical gradients, which can be interrogated to extract predictions about specific interventions that will achieve desired outcomes in vivo.

Emergent behavior of physiological networks can supplement the information available from a fixed genomic sequence. The brain exploited this ancient trick long ago, as neurons and astrocytes use bioelectrical networks to maintain and rewrite stable memories not specified by the genome but rather modified by interactions with the environment (117). We suggest a similar scheme operates in somatic tissues (117). Future work using a combination of computational modeling platforms (116) and transgenic animals that will allow the use of optogenetics (37,38) will facilitate high-resolution studies of planarian bioelectric circuitry, including the specific relationship of voltage states and electrical synapses that determine network topology. The discovery of rewritable pattern memory and accessible stochasticity of large-scale anatomical states enable future efforts to specify the bioelectric code in detail, testing quantitative models of anatomical decision-making that synthesize cell-driven emergence and top-down pattern control (118,119). It remains to be seen whether the paradigms of memory encoding in computational neuroscience (117), and/or other conceptual approaches for understanding cell coordination toward species-specific shapes, will be the key that cracks this fascinating problem.

Our results suggest that it is crucial to pursue the understanding of stable physiological circuits with developmental endpoints, which may provide important sources of epigenetic plasticity and interact with biochemical properties encoded by the genome. Promising avenues for regenerative medicine may lie in manipulating bioelectric physiology for the reestablishment of proper morphology. Many ion transporters are already approved for human clinical use. If bioelectric physiology plays a role in storing morphology, these electroceutical drugs could have promise in reintroducing shape and structure that has been lost. Future work integrating stem cell controls, biochemical networks, and physiological circuits will enable a new depth of understanding of the origin of anatomical form and applications to its rational control.

SUPPORTING MATERIAL

Supporting Materials and Methods, six figures, and one table are available at http://www.biophysj.org/biophysj/supplemental/S0006-3495(17)30427-7.

AUTHOR CONTRIBUTIONS

M.L. and F.D. designed the experiments and interpreted data. F.D., J.M., and K.W. performed the planarian experiments. D.S.A. contributed to the voltage imaging methodology. C.F. created and analyzed the model. F.D., J.M., C.F., D.S.A., and M.L. wrote the manuscript together.

ACKNOWLEDGMENTS

We thank the members of the Levin lab, especially Daniel Lobo for his aid with Fig. 5, and many researchers in the planarian regeneration community for useful discussions. We thank the diligent undergraduates, including Ai Yamasaki, who have helped us tend to our worm colony, as well as Maya Emmons-Bell and Joshua LaPalme for thoughtful discussions and support.

We gratefully acknowledge support by an Allen Discovery Center award from the Paul G. Allen Frontiers Group (No. 12171), the G. Harold and Leila Y. Mathers Charitable Foundation (No. TFU141), the Templeton World Charity Foundation (No. TWCF0089/AB55), and the National Science Foundation (NSF) (Nos. EF-1124651 and IGERT DGE-1144591).

REFERENCES

1. Birnbaum, K. D., and A. Sánchez Alvarado. 2008. Slicing across kingdoms: regeneration in plants and animals. *Cell.* 132:697–710.
2. Losick, R., and C. Desplan. 2008. Stochasticity and cell fate. *Science.* 320:65–68.
3. Somel, M., P. Khaitovich, …, M. Lachmann. 2006. Gene expression becomes heterogeneous with age. *Curr. Biol.* 16:R359–R360.
4. McCaig, C. D., A. M. Rajnicek, …, M. Zhao. 2005. Controlling cell behavior electrically: current views and future potential. *Physiol. Rev.* 85:943–978.
5. McCaig, C. D., A. M. Rajnicek, …, M. Zhao. 2002. Has electrical growth cone guidance found its potential? *Trends Neurosci.* 25:354–359.
6. Funk, R. 2013. Ion gradients in tissue and organ biology (Review). *Biol. Sys. Open Access.* http://dx.doi.org/10.4172/2329-6577.1000105.
7. Bates, E. 2015. Ion channels in development and cancer. *Annu. Rev. Cell Dev. Biol.* 31:231–247.
8. Pullar, C. E. 2011. The Physiology of Bioelectricity in Development, Tissue Regeneration, and Cancer. CRC Press, Boca Raton, FL.
9. Mustard, J., and M. Levin. 2014. Bioelectrical mechanisms for programming growth and form: taming physiological networks for soft body robotics. *Soft Robotics.* 1:169–191.
10. Levin, M. 2014. Molecular bioelectricity: how endogenous voltage potentials control cell behavior and instruct pattern regulation in vivo. *Mol. Biol. Cell.* 25:3835–3850.
11. Jaffe, L. 1982. Developmental currents, voltages, and gradients. *In* Developmental Order: Its Origin and Regulation. S. Subtelny, editor. Alan R. Liss, New York, pp. 183–215.
12. Jaffe, L. F. 1981. The role of ionic currents in establishing developmental pattern. *Philos. Trans. R. Soc. Lond. B Biol. Sci.* 295:553–566.
13. Robinson, K. R. 1985. The responses of cells to electrical fields: a review. *J. Cell Biol.* 101:2023–2027.
14. Jaffe, L. F., and R. Nuccitelli. 1977. Electrical controls of development. *Annu. Rev. Biophys. Bioeng.* 6:445–476.
15. Levin, M., and C. G. Stevenson. 2012. Regulation of cell behavior and tissue patterning by bioelectrical signals: challenges and opportunities for biomedical engineering. *Annu. Rev. Biomed. Eng.* 14:295–323.
16. Tseng, A., and M. Levin. 2013. Cracking the bioelectric code: probing endogenous ionic controls of pattern formation. *Commun. Integr. Biol.* 6:e22595.

17. Lund, E. 1947. Bioelectric Fields and Growth. University of Texas Press, Austin, TX.
18. Burr, H. S., and F. S. C. Northrop. 1935. The electro-dynamic theory of life. *Q. Rev. Biol.* 10:322–333.
19. Becker, R. O. 1967. The electrical control of growth processes. *Med. Times.* 95:657–669.
20. Blackiston, D. J., K. A. McLaughlin, and M. Levin. 2009. Bioelectric controls of cell proliferation: ion channels, membrane voltage and the cell cycle. *Cell Cycle.* 8:3527–3536.
21. Sundelacruz, S., M. Levin, and D. L. Kaplan. 2009. Role of membrane potential in the regulation of cell proliferation and differentiation. *Stem Cell Rev.* 5:231–246.
22. Nuccitelli, R. 2003. A role for endogenous electric fields in wound healing. *Curr. Top. Dev. Biol.* 58:1–26.
23. Reid, B., and M. Zhao. 2014. The electrical response to injury: molecular mechanisms and wound healing. *Adv. Wound Care (New Rochelle).* 3:184–201.
24. Zhao, M. 2009. Electrical fields in wound healing-an overriding signal that directs cell migration. *Semin. Cell Dev. Biol.* 20:674–682.
25. Martin-Granados, C., and C. D. McCaig. 2014. Harnessing the electric spark of life to cure skin wounds. *Adv. Wound Care (New Rochelle).* 3:127–138.
26. Smith, S. D. 1981. The role of electrode position in the electrical induction of limb regeneration in subadult rats. *Bioelectrochem. Bioenerg.* 8:661–670.
27. Smith, S. D. 1974. Effects of electrode placement on stimulation of adult frog limb regeneration. *Ann. N. Y. Acad. Sci.* 238:500–507.
28. Leppik, L. P., D. Froemel, …, J. H. Barker. 2015. Effects of electrical stimulation on rat limb regeneration, a new look at an old model. *Sci. Rep.* 5:18353.
29. Borgens, R. B., J. W. Vanable, Jr., and L. F. Jaffe. 1977. Bioelectricity and regeneration. I. Initiation of frog limb regeneration by minute currents. *J. Exp. Zool.* 200:403–416.
30. Becker, R. O. 1972. Stimulation of partial limb regeneration in rats. *Nature.* 235:109–111.
31. Borgens, R. B. 1984. Are limb development and limb regeneration both initiated by an integumentary wounding? A hypothesis. *Differentiation.* 28:87–93.
32. Jenkins, L. S., B. S. Duerstock, and R. B. Borgens. 1996. Reduction of the current of injury leaving the amputation inhibits limb regeneration in the red spotted newt. *Dev. Biol.* 178:251–262.
33. Adams, D. S., A. Masi, and M. Levin. 2007. H^+ pump-dependent changes in membrane voltage are an early mechanism necessary and sufficient to induce *Xenopus* tail regeneration. *Development.* 134:1323–1335.
34. Tseng, A. S., W. S. Beane, …, M. Levin. 2010. Induction of vertebrate regeneration by a transient sodium current. *J. Neurosci.* 30:13192–13200.
35. Adams, D. S. 2008. A new tool for tissue engineers: ions as regulators of morphogenesis during development and regeneration. *Tissue Eng. Part A.* 14:1461–1468.
36. Chernet, B. T., D. S. Adams, …, M. Levin. 2016. Use of genetically encoded, light-gated ion translocators to control tumorigenesis. *Oncotarget.* 7:19575–19588.
37. Spencer Adams, D., J. M. Lemire, …, M. Levin. 2014. Optogenetics in developmental biology: using light to control ion flux-dependent signals in *Xenopus* embryos. *Int. J. Dev. Biol.* 58:851–861.
38. Adams, D. S., A. S. Tseng, and M. Levin. 2013. Light-activation of the Archaerhodopsin H^+-pump reverses age-dependent loss of vertebrate regeneration: sparking system-level controls in vivo. *Biol. Open.* 2:306–313.
39. Zhao, M., B. Song, …, J. M. Penninger. 2006. Electrical signals control wound healing through phosphatidylinositol-3-OH kinase-γ and PTEN. *Nature.* 442:457–460.
40. Pai, V. P., C. J. Martyniuk, …, M. Levin. 2015. Genome-wide analysis reveals conserved transcriptional responses downstream of resting potential change in *Xenopus* embryos, axolotl regeneration, and human mesenchymal cell differentiation. *Regeneration (Oxf).* 3:3–25.
41. Tseng, A. S., and M. Levin. 2012. Transducing bioelectric signals into epigenetic pathways during tadpole tail regeneration. *Anat. Rec. (Hoboken).* 295:1541–1551.
42. Adams, D. S., S. G. Uzel, …, M. Levin. 2016. Bioelectric signalling via potassium channels: a mechanism for craniofacial dysmorphogenesis in KCNJ2-associated Andersen-Tawil Syndrome. *J Physiol.* 594:3245–3270.
43. Masotti, A., P. Uva, …, B. Dallapiccola. 2015. Keppen-Lubinsky syndrome is caused by mutations in the inwardly rectifying K^+ channel encoded by KCNJ6. *Am. J. Hum. Genet.* 96:295–300.
44. Bando, Y., T. Hirano, and Y. Tagawa. 2014. Dysfunction of KCNK potassium channels impairs neuronal migration in the developing mouse cerebral cortex. *Cereb. Cortex.* 24:1017–1029.
45. Pardo, L. A., and W. Stühmer. 2014. The roles of K^+ channels in cancer. *Nat. Rev. Cancer.* 14:39–48.
46. Becchetti, A. 2011. Ion channels and transporters in cancer. 1. Ion channels and cell proliferation in cancer. *Am. J. Physiol. Cell Physiol.* 301:C255–C265.
47. Djamgoz, M. B., R. C. Coombes, and A. Schwab. 2014. Ion transport and cancer: from initiation to metastasis. *Philos. Trans. R. Soc. Lond. B Biol. Sci.* 369:20130092.
48. Lobikin, M., B. Chernet, …, M. Levin. 2012. Resting potential, oncogene-induced tumorigenesis, and metastasis: the bioelectric basis of cancer in vivo. *Phys. Biol.* 9:065002.
49. Sundelacruz, S., C. Li, …, D. L. Kaplan. 2013. Bioelectric modulation of wound healing in a 3D in vitro model of tissue-engineered bone. *Biomaterials.* 34:6695–6705.
50. Sundelacruz, S., M. Levin, and D. L. Kaplan. 2013. Depolarization alters phenotype, maintains plasticity of predifferentiated mesenchymal stem cells. *Tissue Eng. Part A.* 19:1889–1908.
51. Sundelacruz, S., M. Levin, and D. L. Kaplan. 2008. Membrane potential controls adipogenic and osteogenic differentiation of mesenchymal stem cells. *PLoS One.* 3:e3737.
52. Yasuda, T., and D. J. Adams. 2010. Physiological roles of ion channels in adult neural stem cells and their progeny. *J. Neurochem.* 114:946–959.
53. Liebau, S., A. Kleger, …, S. P. Yu. 2013. Stem cells and ion channels. *Stem Cells Int.* 2013:238635.
54. Sullivan, K. G., M. Emmons-Bell, and M. Levin. 2016. Physiological inputs regulate species-specific anatomy during embryogenesis and regeneration. *Commun. Integr. Biol.* 9:e1192733.
55. Marsh, G., and H. W. Beams. 1952. Electrical control of morphogenesis in regenerating Dugesia tigrina. I. Relation of axial polarity to field strength. *J. Cell. Comp. Physiol.* 39:191–213.
56. Marsh, G., and H. W. Beams. 1950. Electrical control of growth axis in a regenerating annelid. *Anat. Rec.* 108:512.
57. Marsh, G., and H. W. Beams. 1949. Electrical control of axial polarity in a regenerating annelid. *Anat. Rec.* 105:513–514.
58. Marsh, G., and H. W. Beams. 1947. Electrical control of growth polarity in regenerating *Dugesia tigrina*. *Fed. Proc.* 6:163–164.
59. Emmons-Bell, M., F. Durant, …, M. Levin. 2015. Gap junctional blockade stochastically induces different species-specific head anatomies in genetically wild-type *Girardia dorotocephala* flatworms. *Int. J. Mol. Sci.* 16:27865–27896.
60. Beane, W. S., J. Morokuma, …, M. Levin. 2011. A chemical genetics approach reveals H,K-ATPase-mediated membrane voltage is required for planarian head regeneration. *Chem. Biol.* 18:77–89.
61. Beane, W. S., J. Morokuma, …, M. Levin. 2013. Bioelectric signaling regulates head and organ size during planarian regeneration. *Development.* 140:313–322.

62. García-Quismondo, M., M. Levin, and D. Lobo. 2017. Modeling regenerative processes with membrane computing. *Inf. Sci.* 381:229–249.

63. Durant, F., D. Lobo, …, M. Levin. 2016. Physiological controls of large-scale patterning in planarian regeneration: a molecular and computational perspective on growth and form. *Regeneration (Oxf).* 3:78–102.

64. De, A., V. S. Chakravarthy, and M. Levin. 2016. A computational model of planarian regeneration. *Int. J. Parallel Emergent Distributed Syst.* 1–17.

65. Tosenberger, A., N. Bessonov, …, N. Morozova. 2015. A conceptual model of morphogenesis and regeneration. *Acta Biotheor.* 63:283–294.

66. Lobo, D., and M. Levin. 2015. Inferring regulatory networks from experimental morphological phenotypes: a computational method reverse-engineers planarian regeneration. *PLOS Comput. Biol.* 11:e1004295.

67. Levin, M. 2014. Endogenous bioelectrical networks store non-genetic patterning information during development and regeneration. *J. Physiol.* 592:2295–2305.

68. Oviedo, N. J., C. L. Nicolas, D. S. Adams, and M. Levin. 2008. Establishing and maintaining a colony of planarians. *CSH Protoc.* 2008, pdb-prot5053.

69. Nogi, T., and M. Levin. 2005. Characterization of innexin gene expression and functional roles of gap-junctional communication in planarian regeneration. *Dev. Biol.* 287:314–335.

70. Oviedo, N. J., J. Morokuma, …, M. Levin. 2010. Long-range neural and gap junction protein-mediated cues control polarity during planarian regeneration. *Dev. Biol.* 339:188–199.

71. Pearson, B. J., G. T. Eisenhoffer, …, A. Sánchez Alvarado. 2009. Formaldehyde-based whole-mount in situ hybridization method for planarians. *Dev. Dyn.* 238:443–450.

72. Agata, K., Y. Soejima, …, K. Watanabe. 1998. Structure of the planarian central nervous system (CNS) revealed by neuronal cell markers. *Zoolog. Sci.* 15:433–440.

73. Yazawa, S., Y. Umesono, …, K. Agata. 2009. Planarian hedgehog/patched establishes anterior-posterior polarity by regulating Wnt signaling. *Proc. Natl. Acad. Sci. USA.* 106:22329–22334.

74. Nakazawa, M., F. Cebrià, …, T. Gojobori. 2003. Search for the evolutionary origin of a brain: planarian brain characterized by microarray. *Mol. Biol. Evol.* 20:784–791.

75. Cebrià, F., C. Kobayashi, …, K. Agata. 2002. FGFR-related gene nou-darake restricts brain tissues to the head region of planarians. *Nature.* 419:620–624.

76. Reddien, P. W., A. L. Bermange, …, A. Sánchez Alvarado. 2005. Identification of genes needed for regeneration, stem cell function, and tissue homeostasis by systematic gene perturbation in planaria. *Dev. Cell.* 8:635–649.

77. Oviedo, N. J., C. L. Nicolas, D. S. Adams, and M. Levin. 2008. Live imaging of planarian membrane potential using $DiBAC4_3$. *CSH Protoc.* 2008, pdb-prot5055.

78. Dexter, J. P., M. B. Tamme, …, E.-M. S. Collins. 2014. On-chip immobilization of planarians for in vivo imaging. *Sci. Rep.* 4:6388.

79. Özkucur, N., K. P. Quinn, …, D. L. Kaplan. 2015. Membrane potential depolarization causes alterations in neuron arrangement and connectivity in cocultures. *Brain Behav.* 5:24–38.

80. Adams, D. S., and M. Levin. 2012. Measuring resting membrane potential using the fluorescent voltage reporters $DiBAC4_3$ and CC2-DMPE. *Cold Spring Harb. Protoc.* 2012:459–464.

81. Adams, D. S., and M. Levin. 2012. General principles for measuring resting membrane potential and ion concentration using fluorescent bioelectricity reporters. *Cold Spring Harb. Protoc.* 2012:385–397.

82. Epps, D. E., M. L. Wolfe, and V. Groppi. 1994. Characterization of the steady-state and dynamic fluorescence properties of the potential-sensitive dye bis-(1,3-dibutylbarbituric acid)trimethine oxonol (Dibac4(3)) in model systems and cells. *Chem. Phys. Lipids.* 69:137–150.

83. Levin, M., T. Thorlin, …, M. Mercola. 2002. Asymmetries in H^+/K^+-ATPase and cell membrane potentials comprise a very early step in left-right patterning. *Cell.* 111:77–89.

84. Vandenberg, L. N., R. D. Morrie, and D. S. Adams. 2011. V-ATPase-dependent ectodermal voltage and pH regionalization are required for craniofacial morphogenesis. *Dev. Dyn.* 240:1889–1904.

85. Saló, E., J. F. Abril, …, G. Rodríguez-Esteban. 2009. Planarian regeneration: achievements and future directions after 20 years of research. *Int. J. Dev. Biol.* 53:1317–1327.

86. Owlarn, S., and K. Bartscherer. 2016. Go ahead, grow a head! A planarian's guide to anterior regeneration. *Regeneration (Oxf).* 3:139–155.

87. Gentile, L., F. Cebrià, and K. Bartscherer. 2011. The planarian flatworm: an in vivo model for stem cell biology and nervous system regeneration. *Dis. Model. Mech.* 4:12–19.

88. Law, R., and M. Levin. 2015. Bioelectric memory: modeling resting potential bistability in amphibian embryos and mammalian cells. *Theor. Biol. Med. Model.* 12:22.

89. Gallaher, J., M. Bier, and J. S. van Heukelom. 2010. First order phase transition and hysteresis in a cell's maintenance of the membrane potential—an essential role for the inward potassium rectifiers. *Biosystems.* 101:149–155.

90. Pai, V. P., S. Aw, …, M. Levin. 2012. Transmembrane voltage potential controls embryonic eye patterning in *Xenopus laevis*. *Development.* 139:313–323.

91. Mathews, J., and M. Levin. 2016. Gap junctional signaling in pattern regulation: physiological network connectivity instructs growth and form. *Dev. Neurobiol.* 77:643–673.

92. Weingart, R., and F. F. Bukauskas. 1998. Long-chain *n*-alkanols and arachidonic acid interfere with the V_m-sensitive gating mechanism of gap junction channels. *Pflugers Arch.* 435:310–319.

93. Juszczak, G. R., and A. H. Swiergiel. 2009. Properties of gap junction blockers and their behavioural, cognitive and electrophysiological effects: animal and human studies. *Prog. Neuropsychopharmacol. Biol. Psychiatry.* 33:181–198.

94. Morgan, T. 1898. Experimental studies of the regeneration of *Planaria maculata*. *Dev. Genes Evol.* 7:364–397.

95. Morgan, T. H. 1904. The control of heteromorphosis in *Planaria maculata*. *Arch. Entwicklungsmech. Org.* 17:683–694.

96. Petersen, C. P., and P. W. Reddien. 2008. Smed-betacatenin-1 is required for anteroposterior blastema polarity in planarian regeneration. *Science.* 319:327–330.

97. Gurley, K. A., J. C. Rink, and A. Sánchez Alvarado. 2008. β-catenin defines head versus tail identity during planarian regeneration and homeostasis. *Science.* 319:323–327.

98. Sikes, J. M., and P. A. Newmark. 2013. Restoration of anterior regeneration in a planarian with limited regenerative ability. *Nature.* 500:77–80.

99. Liu, S. Y., C. Selck, …, J. C. Rink. 2013. Reactivating head regrowth in a regeneration-deficient planarian species. *Nature.* 500:81–84.

100. Hayashi, T., M. Motoishi, …, H. Tarui. 2011. A LIM-homeobox gene is required for differentiation of Wnt-expressing cells at the posterior end of the planarian body. *Development.* 138:3679–3688.

101. Newmark, P. A., and A. Sánchez Alvarado. 2000. Bromodeoxyuridine specifically labels the regenerative stem cells of planarians. *Dev. Biol.* 220:142–153.

102. Dahal, G. R., J. Rawson, …, E. Bates. 2012. An inwardly rectifying K^+ channel is required for patterning. *Development.* 139:3653–3664.

103. Jang, S. S., J. Park, …, S. J. Kim. 2011. Endothelial progenitor cells functionally express inward rectifier potassium channels. *Am. J. Physiol. Cell Physiol.* 301:C150–C161.

104. Klyubin, I. V., K. M. Kirpichnikova, …, I. A. Gamaley. 2000. The role of reactive oxygen species in membrane potential changes in macrophages and astrocytes. *Membr. Cell Biol.* 13:557–566.

105. Levin, M. 2013. Reprogramming cells and tissue patterning via bioelectrical pathways: molecular mechanisms and biomedical opportunities. *Wiley Interdiscip. Rev. Syst. Biol. Med.* 5:657–676.

106. Levin, M. 2012. Molecular bioelectricity in developmental biology: new tools and recent discoveries: control of cell behavior and pattern formation by transmembrane potential gradients. *BioEssays.* 34:205–217.

107. Forrester, J. V., N. Lois, …, C. McCaig. 2007. The spark of life: the role of electric fields in regulating cell behaviour using the eye as a model system. *Ophthalmic Res.* 39:4–16.

108. Adams, D. S., and M. Levin. 2013. Endogenous voltage gradients as mediators of cell-cell communication: strategies for investigating bioelectrical signals during pattern formation. *Cell Tissue Res.* 352:95–122.

109. Acar, M., J. T. Mettetal, and A. van Oudenaarden. 2008. Stochastic switching as a survival strategy in fluctuating environments. *Nat. Genet.* 40:471–475.

110. Chang, H. H., M. Hemberg, …, S. Huang. 2008. Transcriptome-wide noise controls lineage choice in mammalian progenitor cells. *Nature.* 453:544–547.

111. Lobo, D., M. Solano, …, M. Levin. 2014. A linear-encoding model explains the variability of the target morphology in regeneration. *J. R. Soc. Interface.* 11:20130918.

112. Petersen, C. P., and P. W. Reddien. 2009. Wnt signaling and the polarity of the primary body axis. *Cell.* 139:1056–1068.

113. Turing, A. M. 1952. The chemical basis of morphogenesis. *Philos. Trans. R. Soc. Lond. B Biol. Sci.* 237:37–72.

114. Meinhardt, H. 2007. Computational modelling of epithelial patterning. *Curr. Opin. Genet. Dev.* 17:272–280.

115. Grossberg, S. 2013. Adaptive resonance theory: how a brain learns to consciously attend, learn, and recognize a changing world. *Neural Netw.* 37:1–47.

116. Pietak, A., and M. Levin. 2016. Exploring instructive physiological signaling with the bioelectric tissue simulation engine. *Front. Bioeng. Biotechnol.* 4:55.

117. Pezzulo, G., and M. Levin. 2015. Re-membering the body: applications of computational neuroscience to the top-down control of regeneration of limbs and other complex organs. *Integr. Biol.* 7:1487–1517.

118. Pezzulo, G., and M. Levin. 2016. Top-down models in biology: explanation and control of complex living systems above the molecular level. *J. R. Soc. Interface.* 13:13.

119. Friston, K., M. Levin, …, G. Pezzulo. 2015. Knowing one's place: a free-energy approach to pattern regulation. *J. R. Soc. Interface.* 12:12.

Biophysical Journal, Volume *112*

Supplemental Information

Long-Term, Stochastic Editing of Regenerative Anatomy via Targeting Endogenous Bioelectric Gradients

Fallon Durant, Junji Morokuma, Christopher Fields, Katherine Williams, Dany Spencer Adams, and Michael Levin

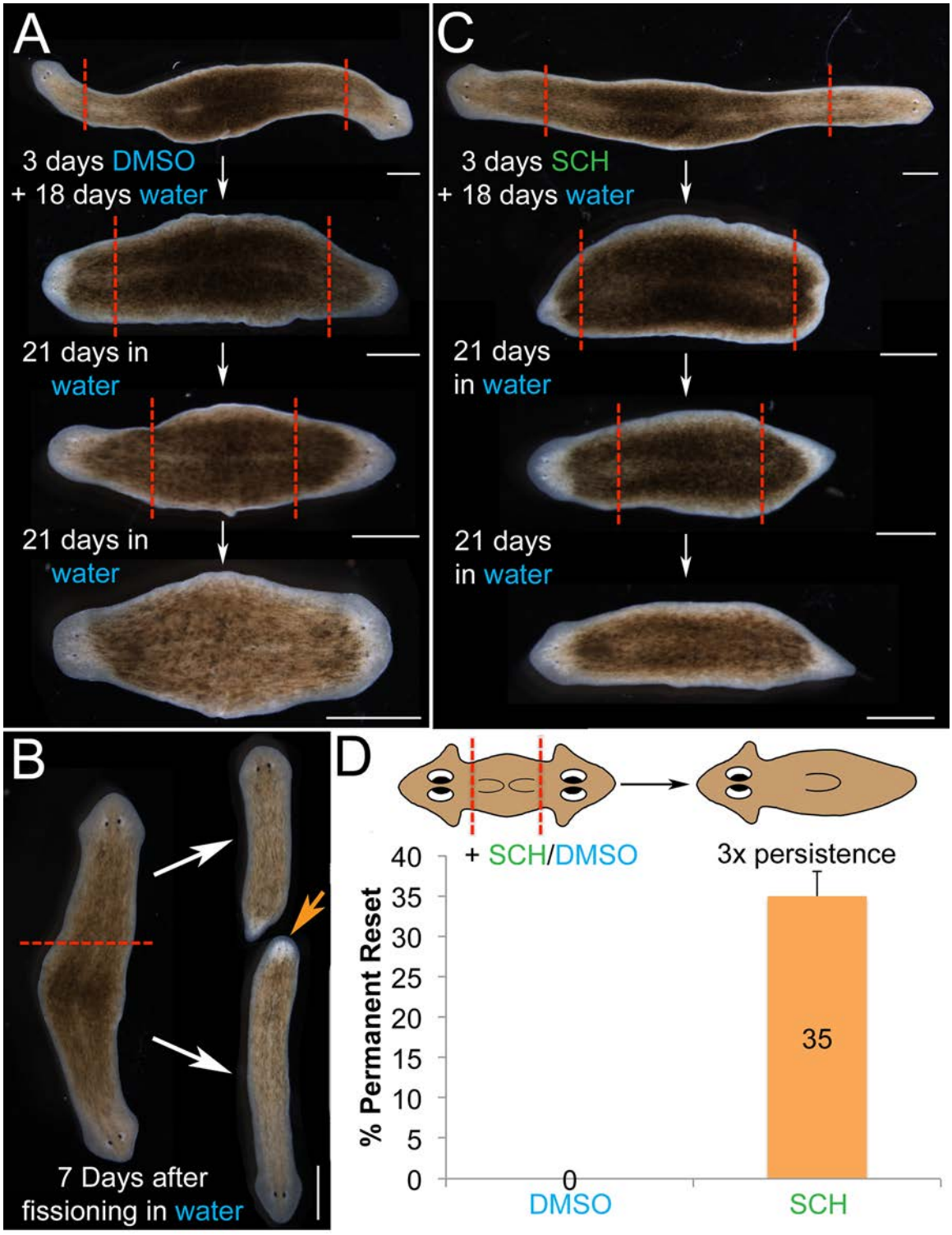

Figure S1: DH phenotype can be reset with bioelectric manipulation.

(A) Planaria that are DH after 8-OH treatment exhibit a permanent change in target morphology. When soaked in only vehicle (DMSO), which does not induce any

patterning defects, recut DH worms regenerate as DH even after three generations of recuts (100%, N=102).

(B) The DH phenotype remains persistent when planaria are allowed to fission on their own, showing that once induced, the phenotype is stable across the most common reproductive mode of this species. Orange arrow indicates second head.

(C) DH, recut, and treated in hyperpolarizing H,K-ATPase inhibitor SCH28080 show a permanent reset of the target morphology back to the SH phenotype (34%, N=102). Similarly, cryptic worms, recut, and treated in SCH28080 show a reduction in the number of DHs regenerated (1%, N=100).

(D) Representation of percent DH that were reset permanently by treatment. Error bars = 95% confidence interval (CIs). Scale bars = 1 mm. SH persisted through three rounds of cutting (34%, N=102), revealing that the change is not to the CRPT (variable) phenotype but to a true, stable WT SH outcome.

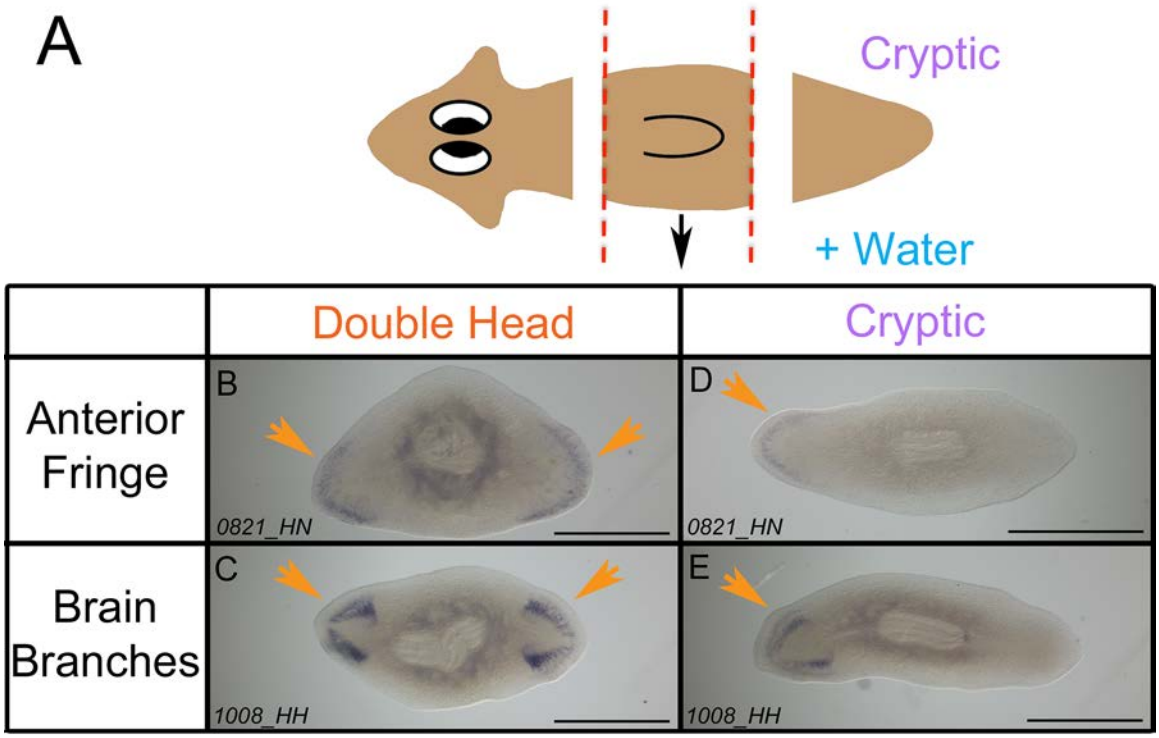

Figure S2: DH worms generated by cutting cryptic worms have true duplicated mature anterior structures.

To confirm that the DH worms indeed have bi-axial anterior structures, tissue specific analyses were performed at 21 days post-amputation (n ≥ 5 for each). (A) Cryptic planaria were cut and allowed to regenerate in water, which produced a population of DH and another population of SH cryptic planaria. (B) The DHs that regenerated from the cryptic planaria exhibit mature chemosensory structures of the anterior fringe (*0821_HN*) (C) as well as mature brain branches (*1008_HH*) on both ends of the planarian (arrowheads), indicating that these planaria are truly DH with complete, mature anterior structures. (D) Resulting SH planaria do not have mature chemosensory structures or (E) mature brain branches in the apparent posterior region of the planarian. Scale bars = 1 mm.

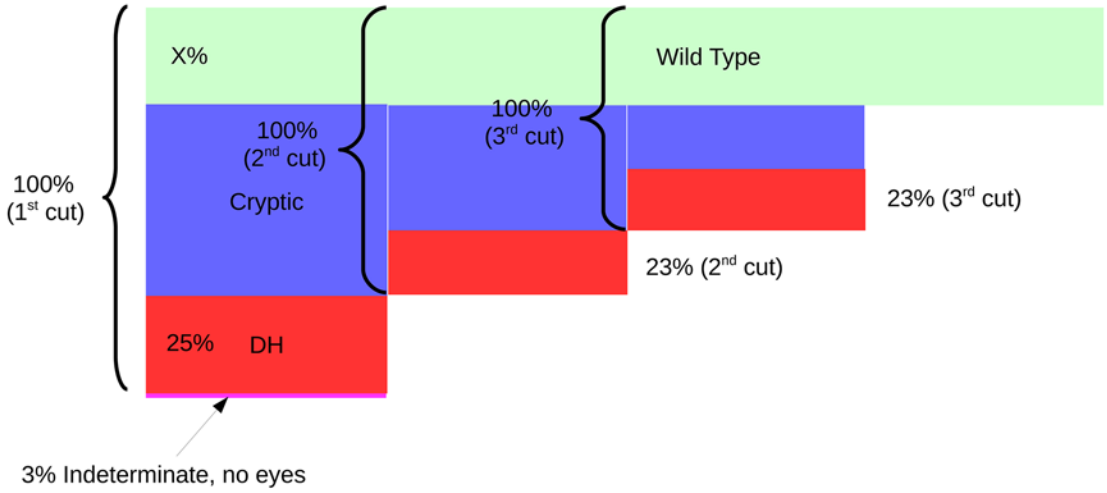

Figure S3: SH regenerates are not WT.

This diagram illustrates in detail why SH regenerates are not WT, by showing the proportion of each type of worm over the first three consecutive cuts. A WT planarian regenerates SH pieces with 100% fidelity. Our experiments show that even normal-looking worms resulting from 8-OH treatment are not truly unaffected, because subsequent cuts result in the same percentage of DH worms, which would never occur if the SH worms were WT. Here we analyze this in more detail, with respect to the dynamics of the three phenotypes in each repeated round of cutting. The null hypothesis is that 8-OH treatment had limited penetrance and SH worms were truly unaffected and remained WT – that a large proportion (X%) of the SH worms will be WT rather than cryptic. This entails that on generation 1 we would have: WT: X%, DH: 25%, Indiscriminate (no eyes): 3%, and Cryptic SH: (72-X)%. Each next round of the experiment is performed on SH worms only, and would contain the assumed X% WT and the (72-X)% cryptics (i.e., 72% of the original population). WT worms do not ever produce DHs when cut in water with no other treatments, so all of the regenerates of WT worms would have to be WT. All the DHs, therefore, must be regenerates of cryptic worms. As this “timecourse” of our experiment illustrates, the fixed WT assumption implies that the fraction of cryptics that regenerate to DH must increase with each generation, even with no additional treatments, which is not observed. Most importantly, after two rounds of amputation in water, our observance of 27% DH from the SH animals is not compatible with the hypothesis that our SH population is WT ($n=30$, $p<0.01$, Fisher’s exact test).

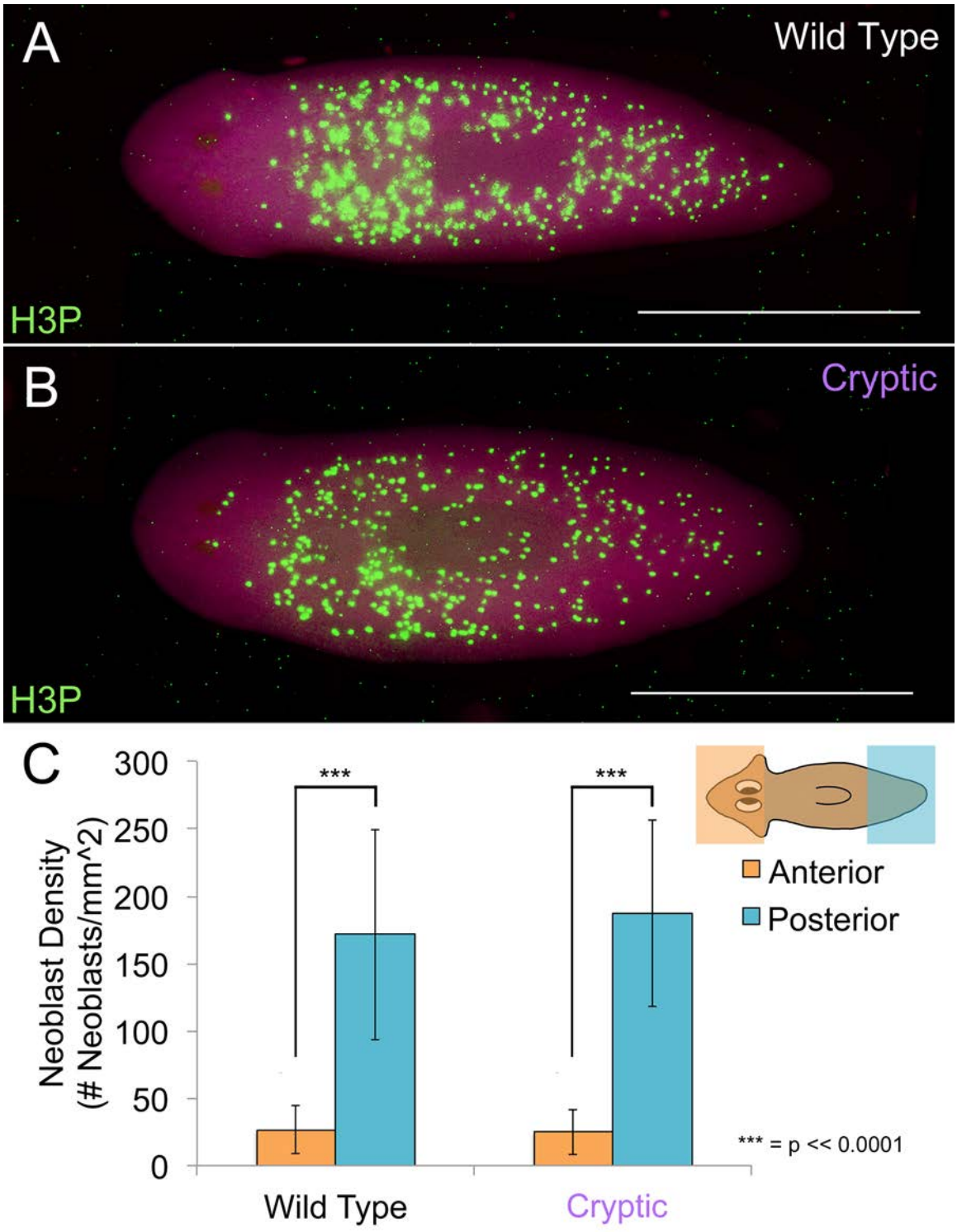

Figure S4: Density of neoblasts in posterior region of cryptic planaria does not resemble anterior neoblast density.

(A-B) WT and cryptic *Dugesia japonica* are devoid of neoblasts (H3P immunohistochemistry) in the region anterior to the eyes. Neoblasts begin immediately posterior to the eyes and extend to the tip of the tail. Neoblasts were counted within a

selection extending to 12% of the total length of the planarian on both anterior and posterior ends using FIJI software ($n \geq 29$) to analyze photos of whole mount transparent worms with all neoblasts and planes visible. Images were threshold adjusted to eliminate background fluorescence. (C) The neoblast density, measured in number of neoblasts/mm^2, was calculated in Excel using FIJI software count and selection area data. Both WT and cryptic planaria showed a significant difference in neoblast density ($p << 0.0001$, two-tailed, unpaired student's t-test) comparing anterior to posterior ends, indicating cryptic tails do not have an anterior-like neoblast distribution. Differences in average neoblast density between WT and cryptic tails are not statistically significant ($p = 0.3369$, two-tailed, unpaired student's t-test) suggesting cryptic tails are more similar to WT tails than heads. Similarly, differences in average neoblast density between WT and cryptic heads are not statistically significant ($p = 0.7813$, two-tailed, unpaired student's t-test). Asterisks = $p << 0.0001$. Error bars = standard deviation. Scale bars = 1 mm.

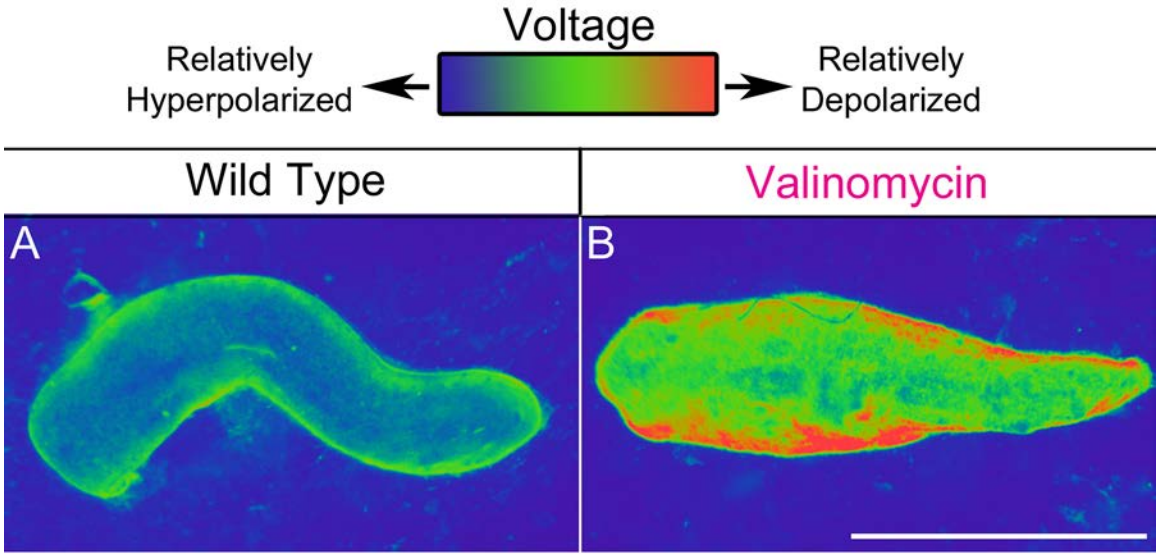

Figure S5: Depolarization via valinomycin + potassium gluconate confirm the ability of DiBAC$_4$(3) to report V$_{mem}$ change

V$_{mem}$ reporter assay using DiBAC$_4$(3) was applied to control vs. depolarizing ionophore-treated worms to confirm that the dye in fact correctly reports V$_{mem}$ change. Images were pseudocolored blue-green-red as with the other dye imaging in this study. Brighter pixels (red) indicate cells that are more relatively depolarized (positively charged) on the inside relative to the outside. Pixels of lower intensity (blue) indicate cells that are more relatively hyperpolarized (negatively charged) on the inside relative to the outside. (A) WT and (B) planaria treated in a 1 µM valinomycin + 150 mM potassium gluconate solution for 1 hour were imaged whole in DiBAC$_4$(3) on a planarian immobilization chip (PIC) (1). Exposure to ionophores depolarizes cells directly, in a much stronger manner than endogenous V$_{mem}$ circuits because they force equalization of positive ions, regardless of the channels or other endogenous bioelectric machinery or cell state. The time course of the experiment had to be very brief because the global depolarization kills the worms rapidly. The DiBAC$_4$(3) fluorescence efficiently reveals the strong depolarizing effects of the ionophore, immediately, even when the worms are not imaged long enough to reveal the endogenous gradients. Upon quantification of intensity values across the whole worm (n = 10 pairs), animals soaked in depolarizing agent were significantly more depolarized than their WT counterparts ($p < 0.05$, unpaired t test), consistent with prior studies using this dye to image voltage (2-11). Scale bars = 1 mm.

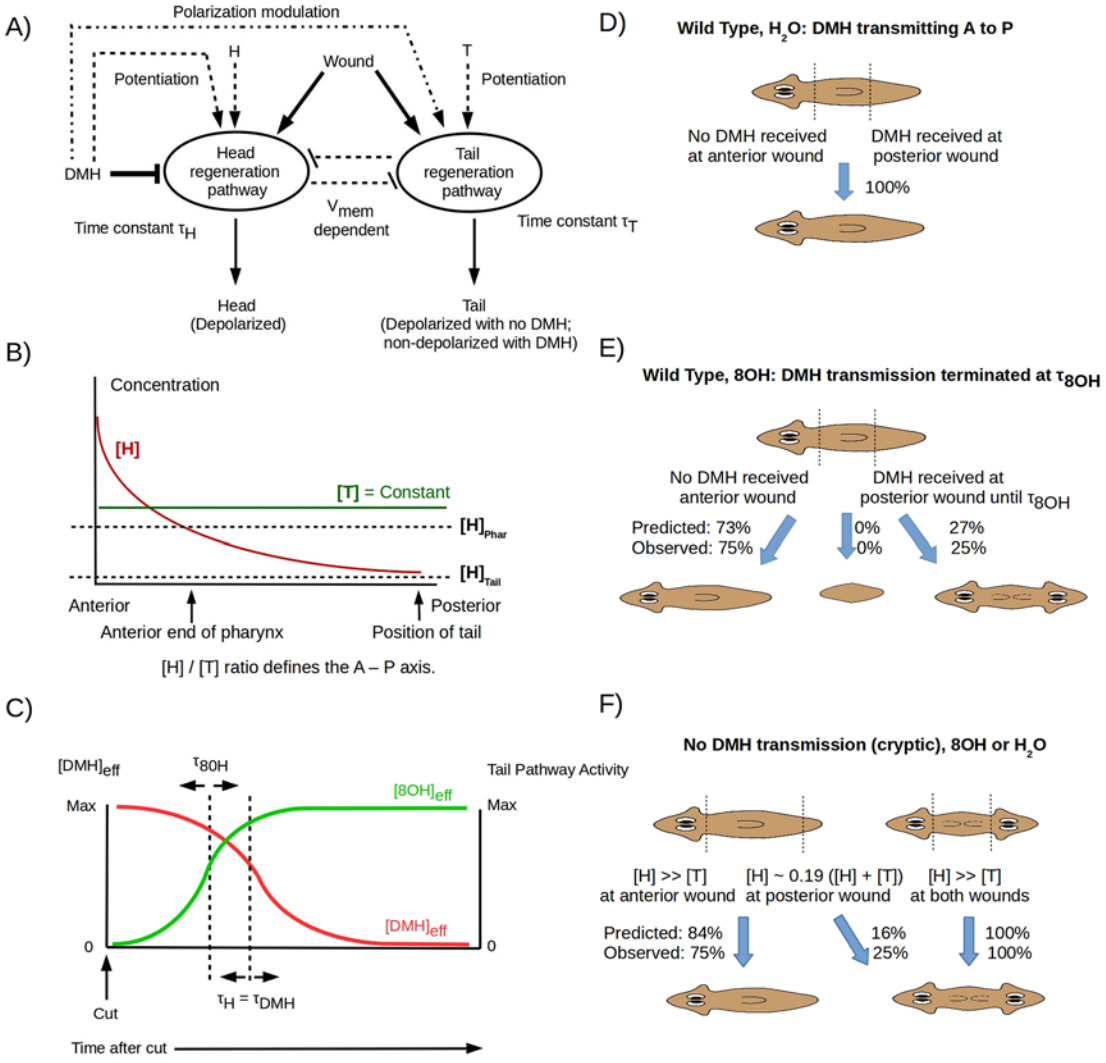

Figure S6: Quantitative model of cryptic–DH branching ratios.

(A) Head and tail regeneration pathways are assumed to be coupled by V_{mem}-dependent mutual inhibition and to both produce depolarized structures by default. Head and tail pathways are quantitatively potentiated by H and T factors, respectively; the head pathway is also potentiated by a "Don't Make Head" (DMH) signal that is actively transmitted in the anterior-to-posterior direction by a V_{mem}- and GJ-dependent mechanism. Wound signal activates potentiated pathways. The DMH signal strongly inhibits the head pathway, and modulates the tail pathway so as to produce a non-depolarized tail. Completed regeneration of head or tail deactivates the head or tail pathway, respectively. The activation time τ_H of the head pathway is shorter than the activation time τ_T of the tail pathway; DMH is assumed to act in a time comparable to τ_H. (B) The ratio of H and T activities, expressible as an effective concentration ratio [H]/[T], decreases along the A/P axis. For simplicity, we assume [H] decreases while [T] remains constant. It is consistent with but not required by the model that [H] = V_{mem}. (C)

The parameter τ_{8OH} / τ_H determines the relation in time between DMH shutoff by 8-OH and inhibition of the head pathway by DMH at the posterior wound. Following DMH shutoff, the head pathway can be activated, producing a DH worm. (D) Simultaneous head and tail amputations of WT animals yield a remnant trunk. No DMH is received at the anterior wound, activating the head pathway. DMH is received at the posterior wound, inhibited the head pathway and allowing the tail pathway to be activated by the wound signal. (E) If head and tail amputation is followed by exposure to 8-OH, the head pathway is initiated normally, in τ_H, at the anterior wound. The head pathway is activated at the posterior wound after τ_{8OH}, i.e. after DMH transmission is shut down, but competes with tail pathway activation during this time. Competition between the pathways produces a stochastic outcome. (F) The morphological outcome of remnant trunk regeneration in cryptic worms with no DMH transmission is determined by the [H]/[T] ratio at the wound sites. See http://chrisfieldsresearch.com/GJ-memory-model.htm for an interactively manipulable version of the model.

Mathematical details of the model

WT worms cut and trunk fragments exposed to 8-OH

At the anterior cut site, anterior-to-posterior DMH transmission is halted immediately. The effective concentration $[DMH]_{eff} = 0$ at the anterior-facing wound of the trunk fragment, allowing the default Head pathway to activate.

At the posterior cut site, anterior-to-posterior DMH transmission continues as long as GJs are operational, inhibiting the Head pathway and allowing Tail pathway activation. Following exposure to 8-OH, DMH transmission stops. The effective transmitted DMH activity thus depends on how soon GJ activity is turned off compared to how fast the Head pathway can activate. Letting τ_{8OH} = time delay from amputation to 8-OH exposure and τ_H = time to activate head pathway, the effective transmitted DMH activity is:

$[DMH]_{sig} = 1/(1 + \exp -10((\tau_{8OH}/\tau_H) – 1.30)))$.

Once DMH transmission is turned off, the residual activity in cells immediately anterior to the posterior wound depends on the posterior cut position x:

$[DMH]_{res} = 1/(1 + \exp 10(x – 0.55))$.

The probability of Head pathway inhibition and hence Tail pathway activation at position x is then:

P_{tail} at $x = [DMH]_{eff}$ at $x = [DMH]_{sig} + [DMH]_{res}$ at x

Normalization gives:

P_{head} at $x = 1 – P_{tail}$ at x

Because $P_{head} = 1$ at the anterior facing wound, the probability of a DH outcome is just P_{head} at the posterior facing wound, i.e. at position x.

Cryptic worms cut and trunk fragments exposed to 8-OH or water

As DMH transmission is off in cryptic worms, the same outcome is expected following exposure to either 8-OH or water. The probability of Head pathway activation then depends only on the ratio of the weak Head (H) and tail (T) factors, which are effectively irrelevant when DMH transmission is active.

For simplicity, we assume that [H] has the same dependence on the posterior cut position as $[DMH]_{res}$ does in a WT animal. In this case, [H] >> [T] at an anterior wound but [H] ~ [T] at a posterior wound. The probability P_{head} at the posterior wound position

x, and hence the probability of a DH outcome, is then just $[DMH]_{res}$ at x scaled by factor representing the relative strengths of the signals:

P_{head} at x = 2.1 $[DMH]_{res}$ at x

Constants in these equations are parameters chosen to fit the x-dependence of the current plus Oviedo *et al.* (2010) data.

Table S1: Cryptic tails are relatively depolarized compared with WT tails

Pair	Wild Type Tail Intensity	Cryptic Tail Intensity	Difference
1	483.8	655.1	171.3
2	396.7	1278.3	881.6
3	619.1	758.4	139.3
4	913.3	1027.2	113.9
5	858.6	1081.3	222.7
6	637.1	1575.8	938.8
7	656.2	2520.1	1863.9
8	762.5	1773.8	1011.3
9	1085.6	1090.7	5.1
10	725.2	752.2	27.0

WT and cryptic planaria were imaged on the same planarian immobilization chip (PIC). Average V_{mem} dye signal intensity was determined via the measure function using FIJI software. A square box proportional to 10% of the total length of the planarian was used to select the most posterior portion of the planarian. Difference between WT and cryptic tail intensity values were calculated using Excel. Each individual cryptic planarian had higher average intensity (relatively depolarized) in the tail region compared to WT and the difference was statistically significant ($p < 0.05$, two-tailed, paired student's t-test). These data represent only those cryptic animals that went on to form DHs. Worms that made SHs upon regeneration were excluded from analysis to enable us to determine what was different about specifically those animals that would change anatomical layout upon cutting.

Supporting References

1. Dexter, J. P., M. B. Tamme, C. H. Lind, and E.-M. S. Collins. 2014. On-chip immobilization of planarians for *in vivo* imaging. *Sci. Rep.* 4.
2. Ozkucur, N., K. P. Quinn, J. C. Pang, C. Du, I. Georgakoudi, E. Miller, M. Levin, and D. L. Kaplan. 2015. Membrane potential depolarization causes alterations in neuron arrangement and connectivity in cocultures. *Brain Behav* 5:24-38.
3. Oviedo, N. J., C. L. Nicolas, D. S. Adams, and M. Levin. 2008. Live Imaging of Planarian Membrane Potential Using $DiBAC_4(3)$. *Cold Spring Harb Protoc* 2008:pdb.prot5055-.
4. Adams, D. S., and M. Levin. 2012. Measuring resting membrane potential using the fluorescent voltage reporters $DiBAC_4(3)$ and CC2-DMPE. *Cold Spring Harbor protocols* 2012:459-464.
5. Adams, D. S., and M. Levin. 2012. General principles for measuring resting membrane potential and ion concentration using fluorescent bioelectricity reporters. *Cold Spring Harbor protocols* 2012:385-397.
6. Epps, D., M. Wolfe, and V. Groppi. 1994. Characterization of the steady-state and dynamic fluorescence properties of the potential-sensitive dye bis-(1,3-dibutylbarbituric acid)trimethine oxonol ($DiBAC_4(3)$) in model systems and cells. *Chem. Phys. Lipids.* 69:137-150.
7. Beane, W. S., J. Morokuma, D. S. Adams, and M. Levin. 2011. A Chemical genetics approach reveals H,K-ATPase-mediated membrane voltage is required for planarian head regeneration. *Chemistry & Biology* 18:77-89.
8. Beane, W. S., J. Morokuma, J. M. Lemire, and M. Levin. 2013. Bioelectric signaling regulates head and organ size during planarian regeneration. *Development* 140:313-322.
9. Adams, D. S., A. Masi, and M. Levin. 2007. H+ pump-dependent changes in membrane voltage are an early mechanism necessary and sufficient to induce Xenopus tail regeneration. *Development* 134:1323-1335.
10. Levin, M., T. Thorlin, K. R. Robinson, T. Nogi, and M. Mercola. 2002. Asymmetries in H+/K+-ATPase and cell membrane potentials comprise a very early step in left-right patterning. *Cell* 111:77-89.
11. Vandenberg, L. N., R. D. Morrie, and D. S. Adams. 2011. V-ATPase-dependent ectodermal voltage and pH regionalization are required for craniofacial morphogenesis. *Dev Dyn* 240:1889-1904.